Analysis and Control of Modular Multilevel Matrix Converters Under Branch Fault Conditions

Chao Wang, *Student Member, IEEE*, Zedong Zheng, *Senior Member, IEEE*, Kui Wang, *Senior Member, IEEE*, Bo Yang, *Member, IEEE*, Peiyi Zhou, *Student Member, IEEE*, and Yongdong Li, *Senior Member, IEEE*

***Abstract*—The modular multilevel matrix converter (M3C) is a promising topology for high-voltage and high-power direct ac-to-ac power conversion applications. Fault tolerance ability is one of the advantages of the M3C. To further enhance the reliability of the M3C, this article proposes a novel branch current configuration method for branch fault conditions, which is available either one or two branches are failed. By deriving basic branch current configurations and analyzing branch dc power equations under branch fault conditions, feasible branch current configurations can be directly derived. In terms of minimizing the maximum peak branch current, the derived configuration is also the optimal one for the single branch fault condition. Compared with the existing method, the proposed method does not need to solve configuration coefficients of branch currents offline, which is automatically adaptive to different load conditions. An M3C prototype with three submodules each branch is built, and experimental results are presented to validate the proposed branch fault tolerance method.**

***Index Terms*—Branch current configuration, branch fault tolerance, energy balance, modular multilevel matrix converter (M3C).**

I. Introduction

MODULAR multilevel topologies present several merits, such as high modularity, easy scalability, high-quality output voltage, and high reliability, which are particularly suitable for high-voltage and high-power applications [1]−[3]. The modular multilevel matrix converter (M3C) is one of these topologies, which is capable of realizing direct ac-to-ac power conversion. It has gained much attention on several applications, such as variable-speed motor drive [4]−[6], low-frequency power transmission [7], [8], offshore wind energy conversion [9]−[11], and pumped hydro storage plants [12]. Reliability is of great importance for these applications. Similar to the widely studied modular multilevel converter (MMC), the M3C is easy to realize SM fault tolerance by configuring redundant submodules (SMs). Several SM open-circuit fault detection and tolerant control methods have been proposed to realize SM fault-tolerant control of the MMC [13]−[15], which are also applicable for the M3C after modification. The operating range of the M3C after SM failures is discussed in [16]. In [16], a neutral point shift method is proposed to maximize the available output voltage and output power of the M3C with a reduced number of SMs, which indicates that the M3C can operate with full input and output voltage range even a limited number of SMs are failed.

Branch failure is more severe and challenging when compared to SM failure. The reason is that branch currents should be reconfigured to maintain desired input and output currents and branch energy balance, since the topology of the converter is changed under branch fault conditions. This kind of fault may be caused by too many failed SMs in one branch, malfunction of SM open-circuit control, mechanical connection failure, etc., [17]−[20]. Among these reasons, too many failed SMs in one branch may be the one with the highest probability of occurrence, which will lead to that the maximum output voltage of the cascade SMs is not enough to support the voltage difference between the input and output side. As a result, the branch current will be out of control. This situation has been considered in [17], an IEEE guide for the application of the MMC in unified power flow controllers in the power grid, which also should be considered for the M3C. Second, according to the experimental results in [15], if the SM is not successfully bypassed after the open-circuit faults of power devices, the branch current and output current will be distorted and the capacitor voltage of the failed SM will keep increasing, which affects the stable and safe operation of the converter. In this case, the branch fault-tolerant control may be needed to enable the converter to operate stably and safely. The mechanical connection failure may mainly be caused by the mechanical stress produced by severe failures of the SM, which can completely disconnect the SM and lead to open circuit of the whole branch.

In [18], control of the single branch failed MMC is analyzed, feasible branch voltage and current configuration are derived by three basic operating constraints of the MMC, i.e., symmetrical output currents, balanced branch energy, and stable dc-link current without fundamental component. However, limited by the maximum output voltage after the fault, this method cannot be applied to the grid-connected MMC. In comparison to the MMC, the M3C can operate with a full range of input and output voltages even though three symmetrical branches are

Manuscript received February 24, 2021; revised June 12, 2021; accepted August 7, 2021. Date of publication August 12, 2021; date of current version October 15, 2021. This work was supported by the National Natural Science Foundation of China under Grant 51777110. Recommended for publication by Associate Editor Y. Yang. *(Corresponding author: Kui Wang.)*

Chao Wang, Zedong Zheng, Kui Wang, Peiyi Zhou, and Yongdong Li are with the State Key Laboratory of Power System, Department of Electrical Engineering ,Tsinghua University, Beijing 100084, China (e-mail: wangchao16@mails.tsinghua.edu.cn; zzd@tsinghua.edu.cn; wangkui@tsinghua.edu.cn; zhoupeiyi@126.com; liyd@mail.tsinghua.edu.cn).

Bo Yang is with the Department of Electrical Engineering, Xi'an University of Technology, Xi'an 710048, China (e-mail: yangbo-xut@163.com).

Color versions of one or more figures in this article are available at https://doi.org/10.1109/TPEL.2021.3104349.

Digital Object Identifier 10.1109/TPEL.2021.3104349

lost [19]. Therefore, the M3C has a certain degree of branch redundancy naturally, which is also an advantage of the M3C in realizing ac-to-ac energy conversion when compared with the back-to-back MMC. But on the other hand, there are more degrees of freedom in the M3C topology. Thus, the branch fault-tolerant control of the M3C is more complex and flexible.

Branch fault tolerance of the M3C is first discussed in [19]. In [19], three branches with symmetrical positions are all removed once one of them fails. As a result, the M3C degenerates to a six-branch topology, which is called the Hexverter. The Hexverter is still a symmetrical topology, and it can operate by employing the branch current configuration proposed in [21]. However, there are two drawbacks of this method. First, since two additional nonfailure branches are removed simultaneously, the remaining branches need to stand larger currents, which leads to a more significant decrement of the power capability under branch fault conditions. Second, the reactive power difference between the input and output system leads to branch energy imbalance. Common-mode voltage (CMV) and circulating current need to be injected into each branch simultaneously to compensate for the energy imbalance. The injection of the CMV raises the maximum branch voltage, resulting in the increment of the voltage stresses on the SM capacitors and power semiconductor devices.

To overcome the two drawbacks, an optimized branch current configuration method is proposed in [20]. In [20], each branch current is expressed as a linear combination of input and output currents in the $\alpha\beta$ reference frame with four coefficients. According to the current constraints at input and output nodes and the constraints of branch energy balance, the relationship between the coefficients of branch currents can be expressed as a series of equality constraints. To determine the optimal branch current configuration, minimizing the quadratic summation of branch current configuration coefficients is selected as the optimization objective. According to the existing equality constraints, the optimal solution is solved by employing the MATLAB solvers offline. This method is validated for different branch fault conditions as long as there are feasible solutions for certain fault conditions. Compared with the strategy proposed in [19], this strategy ensures that the M3C can continue to operate on the condition that only the faulty branches are removed, avoiding the injection of the CMV for different load conditions. However, there are still some shortcomings in this method. First, the optimal branch current configuration cannot be expressed as an analytical expression, which requires to be solved offline for load conditions with different power factors. Therefore, it is necessary to store a lookup table of configuration coefficients in the control chip in advance and switch configuration coefficients according to load power factors online to adapt to different load conditions. Meanwhile, several lookup tables need to be stored for the faults of different branches. As a result, a certain amount of the control chip memory space is occupied, and it is also hard to realize the fine adjustment of the configuration coefficients under different power factors, which is not convenient. Second, it is hard to analyze peak branch currents and capacitor voltage fluctuation rates without analytical expressions of branch currents, which is adverse to analyze the safe operation area (SOA) under branch fault conditions.

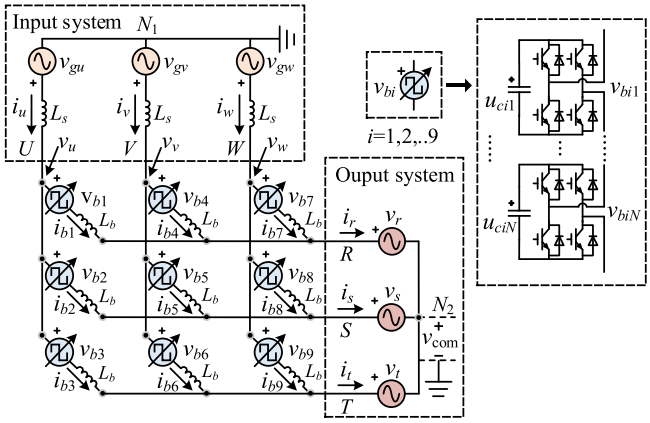

Fig. 1. Circuit topology of the M3C.

To further improve the shortcomings of the method proposed in [20], a novel branch current configuration method is proposed by this article, which separates the determination of the optimal branch current configuration into two steps. The first step is equally allocating the currents of faulty branches to other branches according to the fault conditions. Then, circulating currents are injected in healthy branches to realize branch energy balance in the second step, which can be derived theoretically by solving branch dc power equations. Compared with the existing method, the proposed method can directly derive the analytical branch current configurations adaptive to different load power factors. In terms of minimizing the maximum peak branch current, the derived results are optimal for the single branch fault condition and suboptimal for two branches fault conditions. This article is organized as follows. Section II introduces the proposed branch current configuration method and presents the results for different branch fault conditions. Section III compares the proposed and existing methods. Section IV illustrates the whole control scheme under branch fault conditions. Experimental results presented in Section V verify the validity of the proposed method. Finally, Section VI concludes this article.

II. Branch Fault Analysis and Branch Current Configuration

A. Operating Constraints and Basic Theory of the M3C

The circuit topology of the M3C is shown in Fig. 1, which directly connects two three-phase systems by nine branches (the input and output system are denoted as "UVW" and "RST", respectively). Each branch consists of several cascaded full-bridge SMs and a branch inductor L_b.

Ignoring the voltage drop on the grid-connected inductor L_s, the phase voltage and current of the input side, i.e., v_x and i_x ($x = u, v, w$), and that of the output side, i.e., v_y and i_y ($y = r, s, t$), can be defined as (1). In (1), $\hat{v}_{g1}$ and $\hat{i}_{g1}$ denote the amplitudes of the input voltages and currents, while $\hat{v}_{m2}$ and $\hat{i}_{m2}$ denote that of the output side. φ_1 and φ_2 are the power factor angles of the input and output system, respectively. Generally, input currents are controlled to unity power factor, i.e., $\varphi_1 = 0$, which is a prerequisite for the following analysis of this article. θ is the initial phase angle difference between the voltages of the two

systems

$$\begin{aligned} &v_x \approx v_{gx} = \hat{v}_{g1}\cos\left(\omega_1 t + \alpha_x\right), i_x = \hat{i}_{g1}\cos\left(\omega_1 t - \varphi_1 + \alpha_x\right) \\ &x = u, v, w, \alpha_u = 0, \alpha_v = -2\pi/3, \alpha_w = 2\pi/3 \\ &v_y = \hat{v}_{m2}\cos\left(\omega_2 t + \alpha_y + \theta\right), \\ &i_y = \hat{i}_{m2}\cos\left(\omega_2 t + \alpha_y + \theta - \varphi_2\right) \\ &y = r, s, t, \alpha_r = 0, \alpha_s = -2\pi/3, \alpha_t = 2\pi/3. \end{aligned} \tag{1}$$

Whether in normal or fault conditions, two basic constraints should be satisfied to guarantee the operation and stability of the M3C, which are described as follows.

Constraint 1: The input and output currents should be maintained as desired, which means nine branch currents, i.e., i_{bi} (i = 1, 2,.., 9), need to satisfy Kirchhoff's current law (KCL) at each input and output node. This constraint can be expressed as

$$\begin{aligned} &i_{b1} + i_{b2} + i_{b3} = i_u, i_{b4} + i_{b5} + i_{b6} = i_v, i_{b7} + i_{b8} + i_{b9} = i_w \\ &i_{b1} + i_{b4} + i_{b7} = i_r, i_{b2} + i_{b5} + i_{b8} = i_s, i_{b3} + i_{b6} + i_{b9} = i_t. \end{aligned} \tag{2}$$

Constraint 2: The dc power of each branch should be controlled to 0 to maintain the energy balance of each branch. This constraint can be expressed as (3), where p_{bi}^{dc} is the dc power of branch i and v_{bi} is the output voltage of cascaded SMs in branch i

$$p_{bi}^{\mathrm{dc}} = \overline{v_{bi} \cdot i_{bi}} = 0, i = 1, 2, 3, \ldots, 9. \tag{3}$$

Applying Kirchhoff's voltage law to Fig. 1, the basic mathematical model of the M3C can be described as (4). v_{com} denotes the CMV between the neutral points N_2 and N_1, which equals 0 if no CMV is injected in branch voltages

$$\begin{aligned} &\begin{bmatrix} v_u - v_r & v_v - v_r & v_w - v_r \\ v_u - v_s & v_v - v_s & v_w - v_s \\ v_u - v_t & v_v - v_t & v_w - v_t \end{bmatrix} - v_{\mathrm{com}} \begin{bmatrix} 1 & 1 & 1 \\ 1 & 1 & 1 \\ 1 & 1 & 1 \end{bmatrix} \\ &= L_b \frac{d}{dt} \begin{bmatrix} i_{b1} & i_{b4} & i_{b7} \\ i_{b2} & i_{b5} & i_{b8} \\ i_{b3} & i_{b6} & i_{b9} \end{bmatrix} + \begin{bmatrix} v_{b1} & v_{b4} & v_{b7} \\ v_{b2} & v_{b5} & v_{b8} \\ v_{b3} & v_{b6} & v_{b9} \end{bmatrix}. \end{aligned} \tag{4}$$

When v_{com} is 0 and the voltage drop on L_b is neglected, v_{bi} is approximately equal to the difference of the input and output phase voltage. For example, v_{b1} can be expressed as

$$v_{b1} \approx v_u - v_r. \tag{5}$$

To realize the decouple control of the M3C, double $\alpha\beta 0$ transformation $\mathbf{T}_{2\alpha\beta}$, which is defined as (6) is proposed in [22] and [23]. $\mathbf{T}_{2\alpha\beta}$ is a linear transformation to a certain 3×3 matrix $\mathbf{M}_{3\times3}$

$$\begin{aligned} &\mathbf{T}_{2\alpha\beta}(\mathbf{M}_{3\times3}) = \mathbf{T}_{\alpha\beta} \cdot \mathbf{M}_{3\times3} \cdot {\mathbf{T}_{\alpha\beta}}^{\mathrm{T}} \\ &\mathbf{T}_{\alpha\beta} = \frac{1}{3} \begin{bmatrix} 2 & -1 & -1 \\ 0 & \sqrt{3} & -\sqrt{3} \\ 1 & 1 & 1 \end{bmatrix}. \end{aligned} \tag{6}$$

Appling $\mathbf{T}_{2\alpha\beta}$ to (4), the following equation can be derived:

$$\begin{aligned} \begin{bmatrix} 0 & 0 & -v_\alpha^{rst} \\ 0 & 0 & -v_\beta^{rst} \\ v_\alpha^{uvw} & v_\beta^{uvw} & -v_{\mathrm{com}} \end{bmatrix} &= L_b \frac{d}{dt} \begin{bmatrix} i_{\alpha\alpha} & i_{\alpha\beta} & i_\alpha^{rst}/3 \\ i_{\beta\alpha} & i_{\beta\beta} & i_\beta^{rst}/3 \\ i_\alpha^{uvw}/3 & i_\beta^{uvw}/3 & 0 \end{bmatrix} \\ &+ \begin{bmatrix} v_{\alpha\alpha} & v_{\alpha\beta} & v_{\alpha 0} \\ v_{\beta\alpha} & v_{\beta\beta} & v_{\beta 0} \\ v_{0\alpha} & v_{0\beta} & v_{00} \end{bmatrix} \end{aligned} \tag{7}$$

where $i_{\alpha\alpha}$, $i_{\alpha\beta}$, $i_{\beta\alpha}$, and $i_{\beta\beta}$ are four inner circulating currents of the M3C, which represent four degrees of freedom, which can be independently controlled by corresponding transformed branch voltages, i.e., $v_{\alpha\alpha}$, $v_{\alpha\beta}$, $v_{\beta\alpha}$, and $v_{\beta\beta}$. According to [6], when all circulating currents are controlled to 0, branch currents can be expressed as (8), where $i_{bi(\mathrm{C0})}$ (i = 1,2,..,9) are called the basic branch currents under the normal condition. In this configuration, each branch current consists of one-third corresponding phase current of the input and output side

$$\begin{aligned} &\begin{bmatrix} i_{b1(\mathrm{C0})} & i_{b4(\mathrm{C0})} & i_{b7(\mathrm{C0})} \\ i_{b2(\mathrm{C0})} & i_{b5(\mathrm{C0})} & i_{b8(\mathrm{C0})} \\ i_{b3(\mathrm{C0})} & i_{b6(\mathrm{C0})} & i_{b9(\mathrm{C0})} \end{bmatrix} = \frac{1}{3} \cdot \begin{bmatrix} i_u & i_v & i_w \\ i_u & i_v & i_w \\ i_u & i_v & i_w \end{bmatrix} \\ &+ \frac{1}{3} \cdot \begin{bmatrix} i_r & i_r & i_r \\ i_s & i_s & i_s \\ i_t & i_t & i_t \end{bmatrix}. \end{aligned} \tag{8}$$

It can be proved that this configuration satisfies the two constraints at the same time, and it is an optimal configuration with the minimum quadratic summation of branch current configuration coefficients according to the optimization results in [20]. Therefore, branch currents of the M3C are generally controlled as (8), with small circulating currents injected to compensate for possible branch energy deviation.

One or more branches may fail during the operation of the M3C. As described in [21], the Hexverter, after three symmetrical branches removed, is the simplest topology to connect two three-phase systems. The M3C cannot continue operating after more than three branches are lost. Since the operation of the Hexverter has been detailedly analyzed in [21], this article mainly discusses the control method under one or two branch fault conditions, where the M3C operates asymmetrically.

B. Branch Current Configuration Under Eight-Branch Operating Conditions

When one of nine branches fails, the M3C degenerates to an eight-branch topology. Since each branch of the M3C is rotationally symmetric, the fault of branch 3 is taken as an example, which is shown in Fig. 2. The feasible branch current configuration can be determined by applying the "Constraint 1" and "Constraint 2" step by step.

First, since i_{b3} is 0, current components of i_u and i_t in branch 3 need to be allocated to other branches to guarantee "Constraint 1." A simple allocation method is to evenly allocate current components in i_{b3} to other branches. Therefore, according to the first and the last equations in (2), the current component that equals i_u / 6 + i_t / 6 needs to be injected in i_{b1}, i_{b2}, i_{b6}, and i_{b9}. Then, the current component that equals – i_u / 12 – i_t

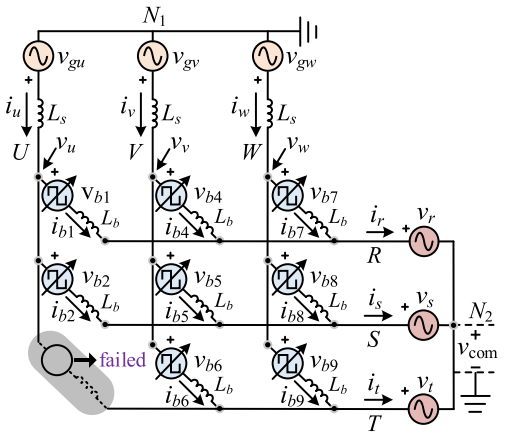

Fig. 2. Circuit configuration when branch 3 is failed.

/ 12 needs to be injected in in i_{b4}, i_{b5}, i_{b7}, and i_{b8} at the same time to guarantee other equations in (2). In order to expand the SOA of the M3C after the branch fault, it is necessary to reduce the current stress on power devices as much as possible, which means the maximum peak branch current, i.e., $\hat{i}_{bi(\max)}$, should be limited as small as possible. However, this allocation may not minimize $\hat{i}_{bi(3\mathrm{F\_max})}$ (The subscript 3F refers to the branch 3 fault condition) when branch 3 is failed. Therefore, based on this allocation, the magnitudes of the additional i_u and i_t components in i_{bi} should be adjusted to obtain a general branch current configuration for optimal analysis. Finally, the general branch current configuration under the branch 3 fault condition, i.e., $i_{bi(3\mathrm{F\_C0})}$, can be expressed as (9), in which the magnitudes of the additional i_u and i_t components in each branch are adjusted by four coefficients a, b, c, and d

$$\begin{cases} i_{b1(3\mathrm{F\_C0})} = \dfrac{i_u}{3} + \dfrac{i_r}{3} + \dfrac{i_u}{6} + \dfrac{i_t}{6} + ai_u + bi_t \\ i_{b2(3\mathrm{F\_C0})} = \dfrac{i_u}{3} + \dfrac{i_s}{3} + \dfrac{i_u}{6} + \dfrac{i_t}{6} - ai_u - bi_t \\ i_{b3(3\mathrm{F\_C0})} = 0 \\ i_{b4(3\mathrm{F\_C0})} = \dfrac{i_v}{3} + \dfrac{i_r}{3} - \dfrac{i_u}{12} - \dfrac{i_t}{12} - \dfrac{(a+c)}{2}i_u - \dfrac{(b+d)}{2}i_t \\ i_{b5(3\mathrm{F\_C0})} = \dfrac{i_v}{3} + \dfrac{i_s}{3} - \dfrac{i_u}{12} - \dfrac{i_t}{12} + \dfrac{(a-c)}{2}i_u + \dfrac{(b-d)}{2}i_t \\ i_{b6(3\mathrm{F\_C0})} = \dfrac{i_v}{3} + \dfrac{i_t}{3} + \dfrac{i_u}{6} + \dfrac{i_t}{6} + ci_u + di_t \\ i_{b7(3\mathrm{F\_C0})} = \dfrac{i_w}{3} + \dfrac{i_r}{3} - \dfrac{i_u}{12} - \dfrac{i_t}{12} - \dfrac{(a-c)}{2}i_u - \dfrac{(b-d)}{2}i_t \\ i_{b8(3\mathrm{F\_C0})} = \dfrac{i_w}{3} + \dfrac{i_s}{3} - \dfrac{i_u}{12} - \dfrac{i_t}{12} + \dfrac{(a+c)}{2}i_u + \dfrac{(b+d)}{2}i_t \\ i_{b9(3\mathrm{F\_C0})} = \dfrac{i_w}{3} + \dfrac{i_t}{3} + \dfrac{i_u}{6} + \dfrac{i_t}{6} - ci_u - di_t. \end{cases} \tag{9}$$

According to (3) and (5), the dc power of fault-free branches under this situation, i.e., $p^{\mathrm{dc}}_{bi(3\mathrm{F\_C0})}$ ($i = 1, 2, 4, \ldots, 9$), can be derived as (10). It is evident that all components in $\mathbf{P}^{\mathrm{dc}}_{(3\mathrm{F\_C0})}$ cannot be controlled to 0 simultaneously only by adjusting the values of a, b, c, and d. Therefore, "Constraint 2" cannot be satisfied when merely employing the branch current configuration expressed by (9).

Although branch 3 is failed, there are still several circulating currents, which can be employed as degrees of freedom to control the energy balance in the eight-branch topology. According to the basic theory of the circuit, for a circuit with b branches and n nodes, the sum of the number of independent circuit loops and independent branches equals $b - n + 1$. Thus, the number of independent circulating currents when branch 3 fails is 3, according to Fig. 2

$$\mathbf{P}^{\mathrm{dc}}_{(3\mathrm{F\_C0})} = \begin{bmatrix} p^{\mathrm{dc}}_{b1(3\mathrm{F\_C0})} \\ p^{\mathrm{dc}}_{b2(3\mathrm{F\_C0})} \\ p^{\mathrm{dc}}_{b4(3\mathrm{F\_C0})} \\ p^{\mathrm{dc}}_{b5(3\mathrm{F\_C0})} \\ p^{\mathrm{dc}}_{b6(3\mathrm{F\_C0})} \\ p^{\mathrm{dc}}_{b7(3\mathrm{F\_C0})} \\ p^{\mathrm{dc}}_{b8(3\mathrm{F\_C0})} \\ p^{\mathrm{dc}}_{b9(3\mathrm{F\_C0})} \end{bmatrix}$$

$$= \begin{bmatrix} (1+4a+2b)\cos\varphi_2/8 - \sqrt{3}(1+6b)\sin\varphi_2/24 \\ (1-4a-2b)\cos\varphi_2/8 + \sqrt{3}(1-6b)\sin\varphi_2/24 \\ (a+c-b-d)\cos\varphi_2/8 + \sqrt{3}\,[1+6(b+d)]\sin\varphi_2/48 \\ (-a+c+b-d)\cos\varphi_2/8 - \sqrt{3}\,[1-6(b-d)]\sin\varphi_2/48 \\ -(1+2c+4d)\cos\varphi_2/8 \\ (a-c-b+d)\cos\varphi_2/8 + \sqrt{3}\,[1+6(b-d)]\sin\varphi_2/48 \\ (-a-c+b+d)\cos\varphi_2/8 - \sqrt{3}\,[1-6(b+d)]\sin\varphi_2/48 \\ (-1+2c+4d)\cos\varphi_2/8 \end{bmatrix}$$

$$\hat{v}_{m2}\hat{i}_{m2}. \tag{10}$$

The branch currents after injecting circulating currents can be expressed as

$$\begin{cases} i_{b1(3\mathrm{F})} = \dfrac{i_u}{3} + \dfrac{i_r}{3} + \dfrac{i_u}{6} + \dfrac{i_t}{6} + ai_u + bi_t + i_{c1} \\ i_{b2(3\mathrm{F})} = \dfrac{i_u}{3} + \dfrac{i_s}{3} + \dfrac{i_u}{6} + \dfrac{i_t}{6} - ai_u - bi_t - i_{c1} \\ i_{b4(3\mathrm{F})} = \dfrac{i_v}{3} + \dfrac{i_r}{3} - \dfrac{i_u}{12} - \dfrac{i_t}{12} - \dfrac{(a+c)}{2}i_u - \dfrac{(b+d)}{2}i_t - \dfrac{i_{c1}+i_{c2}}{2} \\ i_{b5(3\mathrm{F})} = \dfrac{i_v}{3} + \dfrac{i_s}{3} - \dfrac{i_u}{12} - \dfrac{i_t}{12} + \dfrac{(a-c)}{2}i_u + \dfrac{(b-d)}{2}i_t + \dfrac{i_{c1}-i_{c2}}{2} \\ i_{b6(3\mathrm{F})} = \dfrac{i_v}{3} + \dfrac{i_t}{3} + \dfrac{i_u}{6} + \dfrac{i_t}{6} + ci_u + di_t + i_{c2} \\ i_{b7(3\mathrm{F})} = \dfrac{i_w}{3} + \dfrac{i_r}{3} - \dfrac{i_u}{12} - \dfrac{i_t}{12} - \dfrac{(a-c)}{2}i_u - \dfrac{(b-d)}{2}i_t - \dfrac{i_{c1}-i_{c2}}{2} \\ i_{b8(3\mathrm{F})} = \dfrac{i_w}{3} + \dfrac{i_s}{3} - \dfrac{i_u}{12} - \dfrac{i_t}{12} + \dfrac{(a+c)}{2}i_u + \dfrac{(b+d)}{2}i_t + \dfrac{i_{c1}+i_{c2}}{2} \\ i_{b9(3\mathrm{F})} = \dfrac{i_w}{3} + \dfrac{i_t}{3} + \dfrac{i_u}{6} + \dfrac{i_t}{6} - ci_u - di_t - i_{c2}. \end{cases} \tag{11}$$

These equations can be easily derived according to "Constraint 1" and Fig. 2. For instance, when i_{c1} is injected in branch

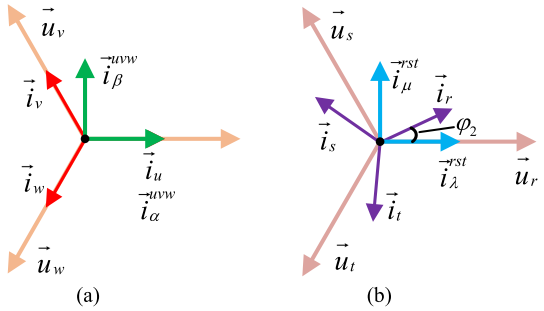

Fig. 3. Directions of the four current components in i_{c1} and i_{c2}. (a) Directions of i_{α}^{uvw} and i_{β}^{uvw}. (b) Directions of i_{λ}^{rst} and i_{μ}^{rst}.

1 to eliminate $p_{b1(3\text{F\_C0})}^{\text{dc}}$, $-i_{c1}$ needs to be injected in branch 2 to ensure "Constraint 1". The same as the injection of i_{c2} in branch 6 and branch 9. For the other four branches, half of i_{c1} and i_{c2} are injected in them considering the symmetry of dc power expression in (10) and the balance of peak branch currents.

According to the orthogonality of the sine function, i_{cj} ($j = 1, 2$) should contain both the input and output fundamental components to realize the energy balance of each branch. For the sake of generality, i_{cj} is defined as (12), which consists of the orthogonal components, which are separately in phase with the α- and β-axis voltage components of the input and output system. The directions of i_{α}^{uvw}, i_{β}^{uvw}, i_{λ}^{rst}, and i_{μ}^{rst} are presented in Fig. 3 for the sake of intuition

$$\begin{aligned} i_{cj} &= k_{j1}\cdot i_{\alpha}^{uvw} + k_{j2}\cdot i_{\beta}^{uvw} + k_{j3}\cdot i_{\lambda}^{rst} + k_{j4}\cdot i_{\mu}^{rst}, j = 1,2 \\ i_{\alpha}^{uvw} &= \hat{i}_{g1}\cos(\omega_1 t), i_{\beta}^{uvw} = \hat{i}_{g1}\sin(\omega_1 t) \\ i_{\lambda}^{rst} &= \hat{i}_{m2}\cos(\omega_2 t+\theta), i_{\mu}^{rst} = \hat{i}_{m2}\sin(\omega_2 t+\theta). \end{aligned} \tag{12}$$

This indicates that feasible branch current configurations are determined by eight coefficients, which can be solved by employing "Constraint 2". The incremental dc power produced by i_{cj} can be derived by multiplying the injected circulating current and branch voltage in each branch, which is denoted in matrix form as (13), where coefficient matrix $\mathbf{A}_{(3\text{F})}$ is given in (15), shown at the bottom of this page

$$\mathbf{\Delta P}_{(3\text{F})}^{\text{dc}} = \mathbf{A}_{(3\text{F})}\mathbf{k}$$

$$\mathbf{\Delta P}_{(3\text{F})}^{\text{dc}} = \left[\Delta p_{b1(3\text{F})}^{\text{dc}}, \Delta p_{b2(3\text{F})}^{\text{dc}}, \Delta p_{b4(3\text{F})}^{\text{dc}}, \ldots, \Delta p_{b9(3\text{F})}^{\text{dc}}\right]^{\text{T}}$$

$$\mathbf{k} = [k_{11}, k_{12}, k_{13}, k_{14}, k_{21}, k_{22}, k_{23}, k_{24}]^{\text{T}}. \tag{13}$$

To ensure "Constraint 2", the incremental dc power should fully offset the original dc power expressed by (10), i.e.,

$$\mathbf{\Delta P}_{(3\text{F})}^{\text{dc}} = -\mathbf{P}_{(3\text{F\_C0})}^{\text{dc}} \Rightarrow \mathbf{A}_{(3\text{F})}\mathbf{k} = -\mathbf{P}_{(3\text{F\_C0})}^{\text{dc}}. \tag{14}$$

According to the basic principle of linear algebra, the solution of (14) depends on the rank of the coefficient matrix $\mathbf{A}_{(3\text{F})}$. When $\cos\varphi_2 \neq 0$, the rank of $\mathbf{A}_{(3\text{F})}$ is 8. Therefore, there is only one set of solutions for (14), which is derived as (16). In (16), $\mathbf{k}_{(3\text{F\_S})}$ is the solution corresponding to the condition when $a = b = c = d = 0$

$$\begin{aligned} \mathbf{k}_{(3\text{F})} &= \mathbf{k}_{(3\text{F\_S})} + \mathbf{k}_{(3\text{F\_}a)} + \mathbf{k}_{(3\text{F\_}b)} + \mathbf{k}_{(3\text{F\_}c)} + \mathbf{k}_{(3\text{F\_}d)} \\ \mathbf{k}_{(3\text{F\_S})} &= \Big[0, 0, \cos\varphi_2/4 - \sqrt{3}\sin\varphi_2/12, -\sqrt{3}\cos\varphi_2/12 \\ &\quad -\sin\varphi_2/4, 0, \sqrt{3}/6, 0, 0\Big]^{\text{T}} \\ \mathbf{k}_{(3\text{F\_}a)} &= a[-1, 0, 0, 0, 0, 0, 0, 0]^{\text{T}} \\ \mathbf{k}_{(3\text{F\_}b)} &= b\Big[0, 0, \cos\varphi_2/2 - \sqrt{3}\sin\varphi_2/2, \sqrt{3}\cos\varphi_2/2 \\ &\quad +\sin\varphi_2/2, 0, 0, 0, 0\Big]^{\text{T}} \\ \mathbf{k}_{(3\text{F\_}c)} &= c[0, 0, 0, 0, -1, 0, 0, 0]^{\text{T}} \\ \mathbf{k}_{(3\text{F\_}d)} &= d\Big[0, -\sqrt{3}/3 + \tan\varphi_2, 0, 0, 0, 0, 0, 2\cos\varphi_2/\sqrt{3}\Big]^{\text{T}}. \end{aligned} \tag{16}$$

As aforementioned, minimizing $\hat{i}_{bi(3\text{F\_max})}$ is employed as the criterion to obtain the optimal circulating current coefficients and branch current configuration. According to (11), branch 1, 2, 6, and 9 present the larger peak branch currents since more fundamental current components are injected in them. Therefore, peak branch currents of them are analyzed, which are derived as (17) and (18). In (17), $k_{13(3\text{F\_S})}$ and $k_{14(3\text{F\_S})}$ are the third and fourth elements in $\mathbf{k}_{(3\text{F\_S})}$

$$\begin{aligned} \hat{i}_{b1(3\text{F})} = \hat{i}_{b2(3\text{F})} &= \sqrt{\frac{1}{4} + \left(\frac{\sqrt{3}}{3} - \tan\varphi_2\right)^2 d^2}\cdot \hat{i}_{g1} \\ &\quad + \sqrt{m^2 + n^2}\cdot \hat{i}_{m2} \\ m &= 1/4 + k_{13(3\text{F\_S})}\cos\varphi_2 + k_{14(3\text{F\_S})}\sin\varphi_2 \\ n &= -\sqrt{3}/12 - k_{13(3\text{F\_S})}\sin\varphi_2 + k_{14(3\text{F\_S})}\cos\varphi_2 \end{aligned}$$

$$\mathbf{A}_{(3\text{F})} = \begin{bmatrix} \cos\varphi_2/2 & 0 & -1/2 & 0 & 0 & 0 & 0 & 0 \\ -\cos\varphi_2/2 & 0 & -1/4 & \sqrt{3}/4 & 0 & 0 & 0 & 0 \\ \cos\varphi_2/8 & -\sqrt{3}\cos\varphi_2/8 & 1/4 & 0 & \cos\varphi_2/8 & -\sqrt{3}\cos\varphi_2/8 & 1/4 & 0 \\ -\cos\varphi_2/8 & \sqrt{3}\cos\varphi_2/8 & 1/8 & -\sqrt{3}/8 & \cos\varphi_2/8 & -\sqrt{3}\cos\varphi_2/8 & -1/8 & \sqrt{3}/8 \\ 0 & 0 & 0 & 0 & -\cos\varphi_2/4 & \sqrt{3}\cos\varphi_2/4 & 1/4 & \sqrt{3}/4 \\ \cos\varphi_2/8 & \sqrt{3}\cos\varphi_2/8 & 1/4 & 0 & -\cos\varphi_2/8 & -\sqrt{3}\cos\varphi_2/8 & -1/4 & 0 \\ -\cos\varphi_2/8 & -\sqrt{3}\cos\varphi_2/8 & 1/8 & -\sqrt{3}/8 & -\cos\varphi_2/8 & -\sqrt{3}\cos\varphi_2/8 & 1/8 & -\sqrt{3}/8 \\ 0 & 0 & 0 & 0 & \cos\varphi_2/4 & \sqrt{3}\cos\varphi_2/4 & -1/4 & -\sqrt{3}/4 \end{bmatrix}\cdot \hat{v}_{m2}\hat{i}_{m2} \tag{15}$$

$$k_{13(3\mathrm{F\_S})} = \cos\varphi_2/4 - \sqrt{3}\sin\varphi_2/12$$
$$k_{14(3\mathrm{F\_S})} = -\sqrt{3}\cos\varphi_2/12 - \sin\varphi_2/4 \quad (17)$$
$$\hat{i}_{b6(3\mathrm{F})} = \sqrt{3}/3\cdot\hat{i}_{g1} + \sqrt{(1/4-gd)^2 + \left(\sqrt{3}/4 - hd\right)^2}\cdot\hat{i}_{m2}$$
$$\hat{i}_{b9(3\mathrm{F})} = \sqrt{3}/3\cdot\hat{i}_{g1} + \sqrt{(1/4+gd)^2 + \left(\sqrt{3}/4 + hd\right)^2}\cdot\hat{i}_{m2}$$
$$g = \left(\frac{2\cos\varphi_2\sin\varphi_2}{\sqrt{3}} - \frac{1}{2}\right), h = \left(\frac{2\cos^2\varphi_2}{\sqrt{3}} - \frac{\sqrt{3}}{2}\right). \quad (18)$$

The variables a, b, and c do not appear in $\hat{i}_{b1(3\mathrm{F})}$, $\hat{i}_{b2(3\mathrm{F})}$, $\hat{i}_{b6(3\mathrm{F})}$, and $\hat{i}_{b9(3\mathrm{F})}$ because the original injected components related to them in (9) are eliminated by the components in i_{c1} and i_{c2}, which are related to $\mathbf{k}_{(3\mathrm{F}\_a)}$, $\mathbf{k}_{(3\mathrm{F}\_b)}$, and $\mathbf{k}_{(3\mathrm{F}\_c)}$ current coefficient matrix, i.e, according to $\mathbf{k}_{(3\mathrm{F})}$ expressed by (16). Since a, b, and c do not have any influence on $\hat{i}_{b1(3\mathrm{F})}$, $\hat{i}_{b2(3\mathrm{F})}$, $\hat{i}_{b6(3\mathrm{F})}$, and $\hat{i}_{b9(3\mathrm{F})}$, they can be set to 0 to simplify the results of $\mathbf{k}_{(3\mathrm{F})}$.

For $\hat{i}_{b1(3\mathrm{F})}$ and $\hat{i}_{b2(3\mathrm{F})}$, it is evident that the maximum value of them is minimum when $d = 0$ since they are increasing functions about $|d|$. While for $\hat{i}_{b6(3\mathrm{F})}$ and $\hat{i}_{b9(3\mathrm{F})}$, two functions can be defined for the second terms of them, i.e., (19), which are functions related to d. Minimizing the maximum value of $\hat{i}_{b6(3\mathrm{F})}$ and $\hat{i}_{b9(3\mathrm{F})}$ is equivalent to minimizing the maximum value of $F_1(d)$ and $F_2(d)$, i.e., $F_{\max}(d)$

$$F_1(d) = (1/4 - g\cdot d)^2 + \left(\sqrt{3}/4 - h\cdot d\right)^2$$
$$= \left(g^2+h^2\right)d^2 - \left[g/2 + \sqrt{3}h/2\right]d + 1/4$$
$$F_2(d) = (1/4 + g\cdot d)^2 + \left(\sqrt{3}/4 + h\cdot d\right)^2$$
$$= \left(g^2+h^2\right)d^2 + \left[g/2 + \sqrt{3}h/2\right]d + 1/4. \quad (19)$$

When $g \neq 0$ or $h \neq 0$, $F_1(d)$ and $F_2(d)$ are quadratic functions, which are symmetric with regard to $d = 0$. Since $F_1(0) = F_2(0)$, $F_{\max}(d)$ is minimum when $d = 0$ according to the basic properties of quadratic function curves, and the minimum value of $F_{\max}(d)$ is 1 / 4. While when $g = h = 0$ (i.e., $\varphi_2 = \pi/6$), $F_1(d)$, and $F_2(d)$ always are equal to 1 / 4 regardless of d, which is the same as the former result.

Therefore, to minimize the maximum value of $\hat{i}_{b6(3\mathrm{F})}$ and $\hat{i}_{b9(3\mathrm{F})}$, the optimal solution is to set $d = 0$, which is coincident with the solution for minimizing the maximum value of $\hat{i}_{b1(3\mathrm{F})}$ and $\hat{i}_{b2(3\mathrm{F})}$. Consequently, the optimal solution to minimize $\hat{i}_{bi(3\mathrm{F\_max})}$ is to set $a = b = c = d = 0$, and the optimal circulating current coefficient matrix, i.e., $\mathbf{k}_{(3\mathrm{F\_opt})}$, is equal to $\mathbf{k}_{(3\mathrm{F\_S})}$ in (16). This proves that the configuration that equally allocates the current components in i_{b3} to other healthy branches is the optimal configuration when branch 3 is failed, which also can be called as the basic branch current configuration under the branch 3 fault condition.

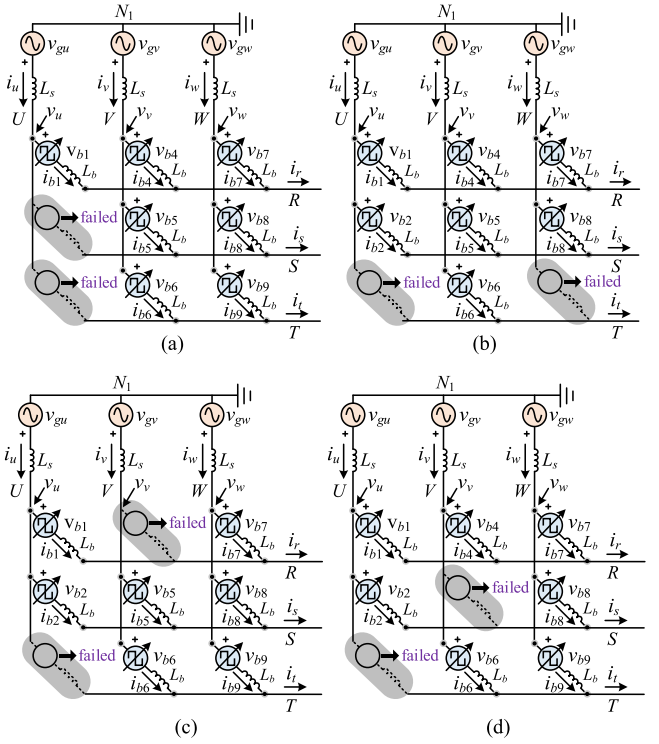

Fig. 4. Four situations when 2 branches are failed in the M3C. (a) Branch 2 and 3 are failed. (b) Branch 3 and 9 are failed. (c) Branch 3 and 4 are failed. (d) Branch 3 and 5 are failed.

When $\cos\varphi_2 = 0$, the rank of $\mathbf{A}_{(3\mathrm{F})}$ changes to 4, there are infinite sets of solutions theoretically. According to the criterion to minimize $\hat{i}_{bi(3\mathrm{F\_max})}$, the optimal solution can be derived as

$$k_{11(3\mathrm{F\_opt})}\big|_{\varphi_2=\pm\pi/2} = 0, k_{12(3\mathrm{F\_opt})}\big|_{\varphi_2=\pm\pi/2} = 0$$
$$k_{13(3\mathrm{F\_opt})}\big|_{\varphi_2=\pm\pi/2} = -\sqrt{3}/12, k_{14(3\mathrm{F\_opt})}\big|_{\varphi_2=\pm\pi/2}$$
$$= -1/4$$
$$k_{21(3\mathrm{F\_opt})}\big|_{\varphi_2=\pm\pi/2} = 0, k_{22(34\mathrm{F\_opt})}\big|_{\varphi_2=\pm\pi/2} = 0$$
$$k_{23(3\mathrm{F\_opt})}\big|_{\varphi_2=\pm\pi/2} = 0, k_{24(3\mathrm{F\_opt})}\big|_{\varphi_2=\pm\pi/2} = 0. \quad (20)$$

Thus far, based on the analysis of "Constraint 1" and "Constraint 2", a feasible and optimal branch current configuration under the branch 3 fault condition is determined. In practical application, $\cos\varphi_2$ and $\sin\varphi_2$ can be calculated online by coordinate transformation according to load voltages and currents. Then, the coefficients of the four current components in i_{c1} and i_{c2} under different load conditions are determined.

C. Branch Current Configuration Under Seven-Branch Operating Conditions

Based on the failure of branch 3, the M3C degenerates into seven-branch topologies if another branch is failed. According to the rotationally symmetric of the M3C, there are four situations, as shown in Fig. 4. The situations in Fig. 4(c) and (d) are treated as two typical fault conditions considering that the relationships between the phase sequence of the input components and that of the output components in two faulty branches are different.

Specifically, the phase sequences of the input and output components in branch 3 and 4 are the same for the case of Fig. 4(c), while the phase sequences of the components in branch 3 and 5 are opposite in Fig. 4(d).

For the first situation, $i_{b1(23\mathrm{F})}$ should be configured as the following to meet "Constraint1":

$$i_{b1(23\mathrm{F})} = i_u. \tag{21}$$

If v_{b1} keeps as (5), the dc power of branch 1 is derived as

$$p^{\mathrm{dc}}_{b1(23\mathrm{F})} = \cos\varphi_2 \cdot \hat{v}_{m2}\hat{i}_{m2}/2. \tag{22}$$

Since there is no circulating current that can be injected in branch 1 according to "Constraint 1", $p^{\mathrm{dc}}_{b1(23\mathrm{F})}$ is unable to be controlled to 0. Therefore, the M3C cannot continue operating under this fault condition unless v_{b1} is also changed, which is not discussed in this article. The same as the second situation.

For the last two situations, branch energy balance is possible to be achieved. The situation when branch 3 and 4 are failed is taken as an example to show the analysis process. According to the analysis of the branch 3 fault condition, the basic branch current configuration under the branch 3 and 4 fault condition can derived as (23) by equally allocating the current components in i_{b3} and i_{b4} to other fault-free branches

$$\begin{cases} i_{b1(34\mathrm{F\_C0})} = i_u/3 + i_r/3 + i_u/6 + i_t/6 + i_v/6 + i_r/6 \\ i_{b2(34\mathrm{F\_C0})} = i_u/3 + i_s/3 + i_u/6 + i_t/6 - i_v/6 - i_r/6 \\ i_{b3(34\mathrm{F\_C0})} = 0 \\ i_{b4(34\mathrm{F\_C0})} = 0 \\ i_{b5(34\mathrm{F\_C0})} = i_v/3 + i_s/3 + i_v/6 + i_r/6 - i_u/6 - i_t/6 \\ i_{b6(34\mathrm{F\_C0})} = i_v/3 + i_t/3 + i_u/6 + i_t/6 + i_v/6 + i_r/6 \\ i_{b7(34\mathrm{F\_C0})} = i_w/3 + i_r/3 + i_v/6 + i_r/6 - i_u/6 - i_t/6 \\ i_{b8(34\mathrm{F\_C0})} = i_w/3 + i_s/3 \\ i_{b9(34\mathrm{F\_C0})} = i_w/3 + i_t/3 + i_u/6 + i_t/6 - i_v/6 - i_r/6. \end{cases} \tag{23}$$

Then, the dc power of fault-free branches under this situation can be expressed as

$$\begin{aligned} \mathbf{P}^{\mathrm{dc}}_{(34\mathrm{F\_N0})} &= \begin{bmatrix} p^{\mathrm{dc}}_{b1(34\mathrm{F\_C0})} \\ p^{\mathrm{dc}}_{b2(34\mathrm{F\_C0})} \\ p^{\mathrm{dc}}_{b5(34\mathrm{F\_C0})} \\ p^{\mathrm{dc}}_{b6(34\mathrm{F\_C0})} \\ p^{\mathrm{dc}}_{b7(34\mathrm{F\_C0})} \\ p^{\mathrm{dc}}_{b8(34\mathrm{F\_C0})} \\ p^{\mathrm{dc}}_{b9(34\mathrm{F\_C0})} \end{bmatrix} \\ &= \begin{bmatrix} -\sqrt{3}\sin\varphi_2/24 \\ \cos\varphi_2/8 + \sqrt{3}\sin\varphi_2/12 \\ \cos\varphi_2/8 - \sqrt{3}\sin\varphi_2/12 \\ \sqrt{3}\sin\varphi_2/24 \\ -\cos\varphi_2/8 + \sqrt{3}\sin\varphi_2/24 \\ 0 \\ -\cos\varphi_2/8 - \sqrt{3}\sin\varphi_2/24 \end{bmatrix} \hat{v}_{m2}\hat{i}_{m2}. \end{aligned} \tag{24}$$

Second, circulating currents should be injected in each fault-free branch to control the dc power to 0. According to Fig. 4, the number of independent circulating currents when branch 3 and 4 fail is 2. Considering "Constraint 1", the branch currents with circulating currents injection are derived as (27) follows:

$$\begin{aligned} &\mathbf{k}_{(34\mathrm{F})} = \mathbf{k}_{(34\mathrm{F\_S})} + \lambda_1\mathbf{k}_{(34\mathrm{F\_B1})} + \lambda_2\mathbf{k}_{(34\mathrm{F\_B2})} \\ &\mathbf{k}_{(34\mathrm{F\_S})} = \Big[1/6, 0, \cos\varphi_2/6 - \sqrt{3}\sin\varphi_2/12, -5\sin\varphi_2/12, 0, \\ &\quad \sqrt{3}/12, -\sqrt{3}\sin\varphi_2/4, -\sqrt{3}\cos\varphi_2/12 + \sin\varphi_2/12\Big]^{\mathrm{T}} \\ &\mathbf{k}_{(34\mathrm{F\_B1})} = \Big[\sqrt{3}/3\cos\varphi_2, -1/\cos\varphi_2, \sqrt{3}/3, 1, 0, 0, 0, 0\Big]^{\mathrm{T}} \\ &\mathbf{k}_{(34\mathrm{F\_B2})} = [0, 0, 0, 0, 1/\cos\varphi_2, 0, 1, 0]^{\mathrm{T}} \end{aligned} \tag{26}$$

$$\mathbf{A}_{(34\mathrm{F})} = \begin{bmatrix} \cos\varphi_2/2 & 0 & -1/2 & 0 & 0 & 0 & 0 & 0 \\ -\cos\varphi_2/2 & 0 & -1/4 & \sqrt{3}/4 & 0 & 0 & 0 & 0 \\ 0 & 0 & 0 & 0 & \cos\varphi_2/4 & -\sqrt{3}\cos\varphi_2/4 & -1/4 & \sqrt{3}/4 \\ 0 & 0 & 0 & 0 & -\cos\varphi_2/4 & \sqrt{3}\cos\varphi_2/4 & 1/4 & \sqrt{3}/4 \\ \cos\varphi_2/4 & \sqrt{3}\cos\varphi_2/4 & 1/2 & 0 & 0 & 0 & 0 & 0 \\ -\cos\varphi_2/4 & -\sqrt{3}\cos\varphi_2/4 & 1/4 & -\sqrt{3}/4 & -\cos\varphi_2/4 & -\sqrt{3}\cos\varphi_2/4 & 1/4 & -\sqrt{3}/4 \\ 0 & 0 & 0 & 0 & \cos\varphi_2/4 & \sqrt{3}\cos\varphi_2/4 & -1/4 & -\sqrt{3}/4 \end{bmatrix} \cdot \hat{v}_{m2}\hat{i}_{m2} \tag{25}$$

$$\begin{cases} i_{b1(34\mathrm{F})} = i_u/3 + i_r/3 + i_u/6 + i_t/6 + i_v/6 + i_r/6 + i_{c1} \\ i_{b2(34\mathrm{F})} = i_u/3 + i_s/3 + i_u/6 + i_t/6 - i_v/6 - i_r/6 - i_{c1} \\ i_{b5(34\mathrm{F})} = i_v/3 + i_s/3 + i_v/6 + i_r/6 - i_u/6 - i_t/6 - i_{c2} \\ i_{b6(34\mathrm{F})} = i_v/3 + i_t/3 + i_u/6 + i_t/6 + i_v/6 + i_r/6 + i_{c2} \\ i_{b7(34\mathrm{F})} = i_w/3 + i_r/3 + i_v/6 + i_r/6 - i_u/6 - i_t/6 - i_{c1} \\ i_{b8(34\mathrm{F})} = i_w/3 + i_s/3 + i_{c1} + i_{c2} \\ i_{b9(34\mathrm{F})} = i_w/3 + i_t/3 + i_u/6 + i_t/6 - i_v/6 - i_r/6 - i_{c2}. \end{cases} \tag{27}$$

The expressions of i_{c1} and i_{c2} are the same as (12). Similar to the aforementioned eight-branch operating condition, the incremental dc power under the branch 3 and 4 fault condition are denoted as (28), where the coefficient matrix $\mathbf{A}_{(34\mathrm{F})}$ is given in (25)

$$\mathbf{\Delta P}^{\mathrm{dc}}_{(34\mathrm{F})} = \mathbf{A}_{(34\mathrm{F})}\mathbf{k}$$

$$\mathbf{\Delta P}^{\mathrm{dc}}_{(34\mathrm{F})} = \left[\Delta p^{\mathrm{dc}}_{b1(34\mathrm{F})}, \Delta p^{\mathrm{dc}}_{b2(34\mathrm{F})}, \Delta p^{\mathrm{dc}}_{b5(34\mathrm{F})}, \ldots, \Delta p^{\mathrm{dc}}_{b9(34\mathrm{F})}\right]^{\mathrm{T}}$$

$$\mathbf{k} = [k_{11}, k_{12}, k_{13}, k_{14}, k_{21}, k_{22}, k_{23}, k_{24}]^{\mathrm{T}}. \tag{28}$$

The "Constraint 2" under this condition can be expressed as

$$\mathbf{\Delta P}^{\mathrm{dc}}_{(34\mathrm{F})} = -\mathbf{P}^{\mathrm{dc}}_{(34\mathrm{F\_C0})} \Rightarrow \mathbf{A}_{(34\mathrm{F})}\mathbf{k} = -\mathbf{P}^{\mathrm{dc}}_{(34\mathrm{F\_C0})}. \tag{29}$$

When $\cos\varphi_2 \neq 0$, the rank of $\mathbf{A}_{(34\mathrm{F})}$ is 6. Therefore, the solution of (29) consists of one special solution of $\mathbf{A}_{(34\mathrm{F})}\mathbf{k} = -\mathbf{P}^{\mathrm{dc}}_{(34\mathrm{F\_C0})}$, i.e., $\mathbf{k}_{(34\mathrm{F\_S})}$, and a linear combination of the two basic solutions of $\mathbf{A}_{(34\mathrm{F})}\mathbf{k} = \mathbf{0}$, i.e., $\mathbf{k}_{(34\mathrm{F\_B1})}$ and $\mathbf{k}_{(34\mathrm{F\_B2})}$, which are derived as (26). In (26), λ_1 and λ_2 are utilized to represent the linear combination of $\mathbf{k}_{(34\mathrm{F\_B1})}$ and $\mathbf{k}_{(34\mathrm{F\_B2})}$, which can be arbitrary values. It is evident that $\mathbf{k}_{(34\mathrm{F\_B1})}$ is only related to the coefficients of i_{c1} while $\mathbf{k}_{(34\mathrm{F\_B2})}$ is only related to the coefficients of i_{c2}.

Different from the branch 3 fault condition, the expressions of peak branch currents under the branch 3 and 4 fault condition, i.e., $\hat{i}_{bi(34\mathrm{F})}$, are relatively complex. The general expression of $\hat{i}_{bi(34\mathrm{F})}$ can be defined as (30), where $K_{bi\_1(34\mathrm{F})}$ and $K_{bi\_2(34\mathrm{F})}$ are the magnitudes of the input and output current components in $i_{bi(34\mathrm{F})}$. $K_{bi\_1(34\mathrm{F})}$ and $K_{bi\_2(34\mathrm{F})}$ can be calculated according to (26) and (27)

$$\hat{i}_{bi(34\mathrm{F})} = K_{bi\_1(34\mathrm{F})}\hat{i}_{g1} + K_{bi\_2(34\mathrm{F})}\hat{i}_{m2}, K_{bi\_1(34\mathrm{F})} \quad K_{bi\_2(34\mathrm{F})} > 0. \tag{30}$$

Considering $K_{bi\_1(34\mathrm{F})}$ and $K_{bi\_2(34\mathrm{F})}$ may be related to λ_1 or λ_2 simultaneously, the maximum value of $\hat{i}_{bi(34\mathrm{F})}$ and corresponding optimal λ_1 and λ_2 are also related to $\hat{i}_{g1}/\hat{i}_{m2}$. Generally, parameters of power components in the M3C are designed on the condition where $\hat{v}_{g1} = \hat{v}_{m2}$. According to the active power balance between the input and output side, the relationship between $\hat{i}_{g1}$and $\hat{i}_{m2}$ can be expressed as $\hat{i}_{g1} = \hat{i}_{m2}|\cos\varphi_2|$ on this condition, which is employed to calculate $\hat{i}_{bi(34\mathrm{F})}$.

According to (27) and the results of $\mathbf{k}_{(34\mathrm{F\_B1})}$ and $\mathbf{k}_{(34\mathrm{F\_B2})}$, $\hat{i}_{b1(34\mathrm{F})}$, $\hat{i}_{b2(34\mathrm{F})}$, and $\hat{i}_{b7(34\mathrm{F})}$ are only related to λ_1, while $\hat{i}_{b5(34\mathrm{F})}$, $\hat{i}_{b6(34\mathrm{F})}$, and $\hat{i}_{b9(34\mathrm{F})}$ are only related to λ_2. Therefore, the maximum one of $\hat{i}_{b1(34\mathrm{F})}$, $\hat{i}_{b2(34\mathrm{F})}$, and $\hat{i}_{b7(34\mathrm{F})}$, i.e., $\hat{i}_{b\max1(34\mathrm{F})}$, and that of $\hat{i}_{b5(34\mathrm{F})}$, $\hat{i}_{b6(34\mathrm{F})}$, and $\hat{i}_{b9(34\mathrm{F})}$, i.e., $\hat{i}_{b\max2(34\mathrm{F})}$ are employed to analyze the optimal λ_1 and λ_2, respectively. Considering the magnitudes of fundamental current components in branch 8 are less than that in other branches, $\hat{i}_{b8(34\mathrm{F})}$ does not need to be considered. Since the expressions of $K_{bi\_1(34\mathrm{F})}$ and $K_{bi\_2(34\mathrm{F})}$ are relatively complex, the analytical optimal results of λ_1 and λ_2 are challenging to be derived. As a result, curves of $\hat{i}_{bi(34\mathrm{F})}$, $\hat{i}_{b\max1(34\mathrm{F})}$, and $\hat{i}_{b\max2(34\mathrm{F})}$ under different φ_2 are presented in Figs. 5 and 6 to assist the analysis, where the minimum values of $\hat{i}_{b\max1(34\mathrm{F})}$ and $\hat{i}_{b\max2(34\mathrm{F})}$ under the optimal λ_1 and λ_2 (i.e., λ_{1_opt} and λ_{2_opt}) and the values when λ_1 and λ_2 are equal to 0 are also presented. As shown in Figs. 5 and 6, the optimal values of λ_1 and λ_2 change along with φ_2. Meanwhile, although the values of $\hat{i}_{b\max1(34\mathrm{F})}$ and $\hat{i}_{b\max2(34\mathrm{F})}$ at $\lambda_1 = 0$ and $\lambda_2 = 0$ are not minimum, they are not much larger than their minimum values. Considering the optimal

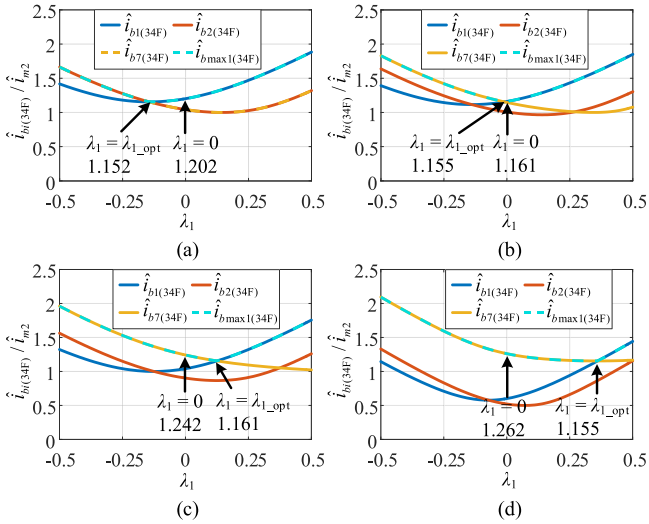

Fig. 5. Curves of $\hat{i}_{b1(34\mathrm{F})}$, $\hat{i}_{b2(34\mathrm{F})}$, $\hat{i}_{b7(34\mathrm{F})}$, and $\hat{i}_{b\max1(34\mathrm{F})}$ along with λ_1 under different φ_2. (a) $\varphi_2 = 0$. (b) $\varphi_2 = \pi/12$. (c) $\varphi_2 = \pi/6$. (d) $\varphi_2 = \pi/3$.

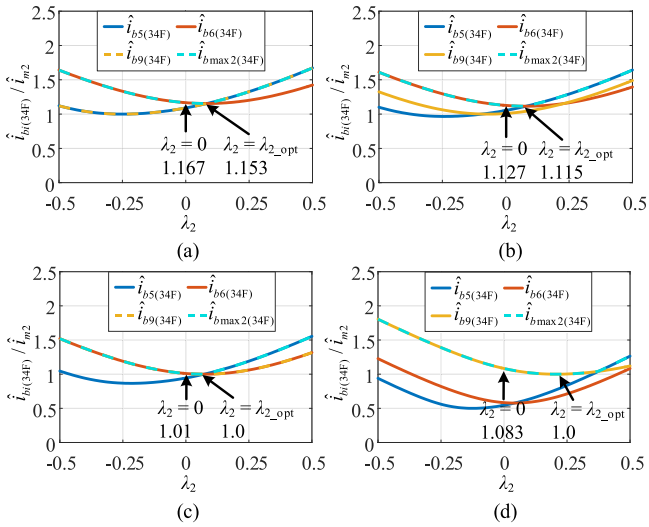

Fig. 6. Curves of $\hat{i}_{b5(34\mathrm{F})}$, $\hat{i}_{b6(34\mathrm{F})}$, $\hat{i}_{b9(34\mathrm{F})}$, and $\hat{i}_{b\max2(34\mathrm{F})}$ along with λ_2 under different φ_2. (a) $\varphi_2 = 0$. (b) $\varphi_2 = \pi/12$. (c) $\varphi_2 = \pi/6$. (d) $\varphi_2 = \pi/3$.

λ_1 and λ_2 are difficult to be expressed by analytical expressions, the branch current configuration when setting $\lambda_1 = \lambda_2 = 0$ is a simple and suboptimal one. Therefore, this configuration is selected to realize the operation under the branch 3 and 4 fault condition, and the selected circulating current coefficient matrix, i.e., $\mathbf{k}_{(34\mathrm{F\_sel})}$, is equal to $\mathbf{k}_{(34\mathrm{F\_S})}$ in (26).

In addition, it is also possible to solve the optimization problem of minimizing $\hat{i}_{b\max 1(34\mathrm{F})}$ and $\hat{i}_{b\max 2(34\mathrm{F})}$ offline to obtain the optimal λ_1 and λ_2 under different φ_2 and store the optimal results as a look-up table to determine the optimal branch current configuration.

When $\cos\varphi_2 = 0$, the rank of $\mathbf{A}_{(34\mathrm{F})}$ changes to 4, the selected coefficients are

$$\begin{aligned}
&k_{11(34\mathrm{F_sel})}\big|_{\varphi_2=\pm\pi/2} = 0, k_{12(34\mathrm{F_sel})}\big|_{\varphi_2=\pm\pi/2} = 0\\
&k_{13(34\mathrm{F_sel})}\big|_{\varphi_2=\pm\pi/2} = -\sqrt{3}/12, k_{14(34\mathrm{F_sel})}\big|_{\varphi_2=\pm\pi/2} = -5/12\\
&k_{21(34\mathrm{F_sel})}\big|_{\varphi_2=\pm\pi/2} = 0, k_{22(34\mathrm{F_sel})}\big|_{\varphi_2=\pm\pi/2} = 0\\
&k_{23(34\mathrm{F_sel})}\big|_{\varphi_2=\pm\pi/2} = -\sqrt{3}/4, k_{24(34\mathrm{F_sel})}\big|_{\varphi_2=\pm\pi/2} = 1/12.
\end{aligned} \tag{31}$$

For the situation when branch 3 and 5 are failed, the selected branch current configuration can also be derived by the same approach as the branch 3 and 4 fault condition. The derived results and selected circulating current coefficients are expressed as follows:

$$\begin{cases}
i_{b1(35\mathrm{F})} = i_u/3 + i_r/3 + i_u/6 + i_t/6 - i_v/6 - i_s/6 + i_{c1}\\
i_{b2(35\mathrm{F})} = i_u/3 + i_s/3 + i_u/6 + i_t/6 + i_v/6 + i_s/6 - i_{c1}\\
i_{b4(35\mathrm{F})} = i_v/3 + i_r/3 + i_v/6 + i_s/6 - i_u/6 - i_t/6 - i_{c2}\\
i_{b6(35\mathrm{F})} = i_v/3 + i_t/3 + i_u/6 + i_t/6 + i_v/6 + i_s/6 + i_{c2}\\
i_{b7(35\mathrm{F})} = i_w/3 + i_r/3 - i_{c1} + i_{c2}\\
i_{b8(35\mathrm{F})} = i_w/3 + i_s/3 + i_v/6 + i_s/6 - i_u/6 - i_t/6 + i_{c1}\\
i_{b9(35\mathrm{F})} = i_w/3 + i_t/3 + i_u/6 + i_t/6 - i_v/6 - i_s/6 - i_{c2}
\end{cases} \tag{32}$$

$$\begin{aligned}
&k_{11(35\mathrm{F_sel})} = -1/6, k_{12(35\mathrm{F_sel})} = 0\\
&k_{13(35\mathrm{F_sel})} = \cos\varphi_2/12 - \sqrt{3}\sin\varphi_2/6\\
&k_{14(35\mathrm{F_sel})} = -\sqrt{3}\cos\varphi_2/12 - \sin\varphi_2/3\\
&k_{21(35\mathrm{F_sel})} = 0, k_{22(35\mathrm{F_sel})} = \sqrt{3}/12\\
&k_{23(35\mathrm{F_sel})} = -\cos\varphi_2/8 - \sqrt{3}\sin\varphi_2/6\\
&k_{24(35\mathrm{F_sel})} = -\sqrt{3}\cos\varphi_2/24 + \sin\varphi_2/3.
\end{aligned} \tag{33}$$

For the situation when $\cos\varphi_2 = 0$, the selected coefficients are

$$\begin{aligned}
&k_{11(35\mathrm{F_sel})}\big|_{\varphi_2=\pm\pi/2} = 0, k_{12(35\mathrm{F_sel})}\big|_{\varphi_2=\pm\pi/2} = 0\\
&k_{13(35\mathrm{F_sel})}\big|_{\varphi_2=\pm\pi/2} = -\sqrt{3}/6, k_{14(35\mathrm{F_sel})}\big|_{\varphi_2=\pm\pi/2} = -1/3\\
&k_{21(35\mathrm{F_sel})}\big|_{\varphi_2=\pm\pi/2} = 0, k_{22(35\mathrm{F_sel})}\big|_{\varphi_2=\pm\pi/2} = 0\\
&k_{23(35\mathrm{F_sel})}\big|_{\varphi_2=\pm\pi/2} = -\sqrt{3}/6, k_{24(35\mathrm{F_sel})}\big|_{\varphi_2=\pm\pi/2} = 1/3.
\end{aligned} \tag{34}$$

III. Comparison Between the Proposed and Existing Method

For the existing method proposed in [20], each branch current is expressed as a linear combination of input and output currents with four coefficients, i.e.,

$$\begin{aligned}
&i_{bi} = p_{i1}\cdot i_\alpha^{uvw} + p_{i2}\cdot i_\beta^{uvw} + p_{i3}\cdot i_\alpha^{rst} + p_{i4}\cdot i_\beta^{rst},\\
&\qquad i = 1, 2, 3, \ldots 9\\
&i_\alpha^{rst} = \hat{i}_{m2}\cos(\omega_2 t + \theta - \varphi_2), i_\beta^{rst} = \hat{i}_{m2}\sin(\omega_2 t + \theta - \varphi_2).
\end{aligned} \tag{35}$$

i_α^{rst} and i_β^{rst} are the α- and β-axis components of the output currents, which are in different directions with i_λ^{rst} and i_μ^{rst} in (12) unless $\cos\varphi_2 = 1$.

The branch 3 fault condition is taken as an example to compare the two methods. For the method proposed in [20], the coefficients of branch 3 are set to 0 automatically. Then, "Constraint 1" and "Constraint 2" are expressed by 24 and 8 equations, respectively. Finally, the following equation is selected as the optimization objective to determine the optimal branch current configuration, which is an optimization model with 32 coefficients and 32 equality constraints:

$$\mathrm{Minimize} J = \sum_{i=1}^{9}\sum_{m=1}^{4} p_{im}^2. \tag{36}$$

The optimal coefficient matrix $[p_{im}]_{(\mathrm{EM})}$ (m = 1, 2, 3, 4) under the load condition when φ_2 is 7.2° is presented in [20], which is

$$[p_{im}]_{(\mathrm{EM})} = \begin{bmatrix}
0.512 & 0 & 0.4709 & -0.327\\
0.488 & 0 & -0.4709 & 0.327\\
0 & 0 & 0 & 0\\
-0.256 & 0.1339 & 0.2645 & 0.1635\\
-0.244 & 0.1548 & -0.0145 & 0.2695\\
0 & 0.5774 & -0.25 & -0.433\\
-0.256 & -0.1339 & 0.2645 & 0.1635\\
-0.244 & -0.1548 & -0.0145 & 0.2695\\
0 & -0.5774 & -0.25 & -0.433
\end{bmatrix}. \tag{37}$$

The optimal results derived by the proposed method in (11), (12), and (16) can be converted into the form of (35). The converted coefficient matrix $[p_{im}]_{(\mathrm{PM})}$ is

$$[p_{im}]_{(\mathrm{PM})} = \begin{bmatrix}
0.5 & 0 & 0.4562 & -0.3463\\
0.5 & 0 & -0.4562 & 0.3463\\
0 & 0 & 0 & 0\\
-0.25 & 0.1433 & 0.2719 & 0.17315\\
-0.25 & 0.1433 & -0.0219 & 0.25985\\
0 & 0.5774 & -0.25 & -0.433\\
-0.25 & -0.1433 & 0.2719 & 0.17315\\
-0.25 & -0.1433 & -0.0219 & 0.25985\\
0 & -0.5774 & -0.25 & -0.433
\end{bmatrix}. \tag{38}$$

The values of J when employing the existing and proposed method, i.e., $J_{(\mathrm{EM})}$ and $J_{(\mathrm{PM})}$, can be calculated as

$$J_{(\mathrm{EM})} = 2.9974, J_{(\mathrm{PM})} = 2.9988. \tag{39}$$

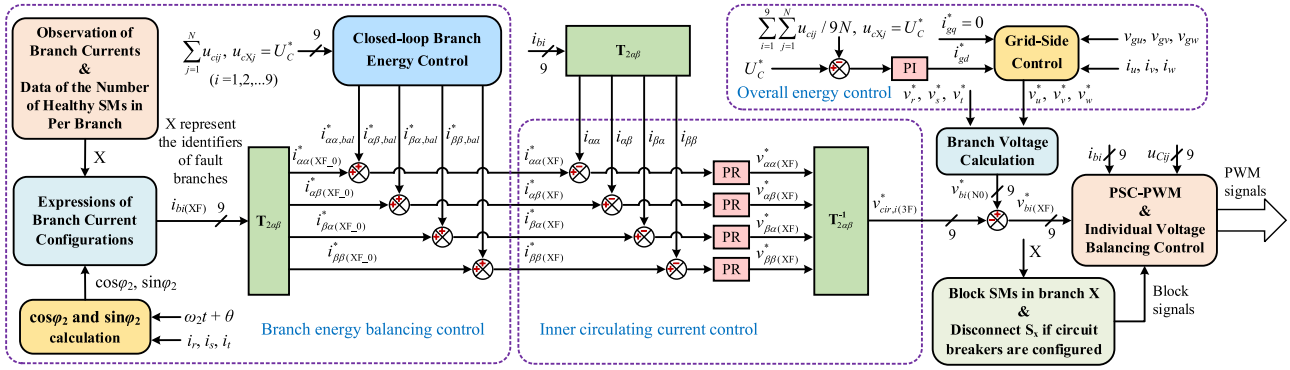

Fig. 7. Whole control scheme of the M3C under branch fault conditions.

It can be seen that although the method of [20] ensures minimum J by solving the quadratic optimization problem, $J_{(\mathrm{PM})}$ is only 0.047% larger than $J_{(\mathrm{EM})}$, which present little difference. Actually, (36) partly represents the summation of the peak branch currents. However, in terms of minimizing $\hat{i}_{bi(\max)}$, the optimization result obtained from (36) is not necessarily the optimal one. Assuming $\hat{v}_{g1} = \hat{v}_{m2}$ under this load condition, the peak branch current in unit form can be expressed as

$$\hat{i}_{bi\_pu} = \sqrt{p_{i1}^2 + p_{i2}^2}\cos\varphi_2 + \sqrt{p_{i3}^2 + p_{i4}^2}. \tag{40}$$

The maximum value of $\hat{i}_{bi\_pu}$ for the existing and proposed method, i.e., $\hat{i}_{bi\_pu(\max\_\mathrm{EM})}$ and $\hat{i}_{bi\_pu(\max\_\mathrm{PM})}$, can be calculated as

$$\begin{aligned} \hat{i}_{bi\_pu(\max\_\mathrm{EM})} &= \hat{i}_{b1\_pu(\mathrm{EM})} = 1.0813 \\ \hat{i}_{bi\_pu(\max\_\mathrm{PM})} &= \hat{i}_{b6\_pu(\mathrm{PM})} = 1.0728. \end{aligned} \tag{41}$$

It can be seen that $\hat{i}_{bi\_pu(\max\_\mathrm{EM})}$ is 0.8% larger than $\hat{i}_{bi\_pu(\max\_\mathrm{PM})}$. This is in coincidence with the theoretical analysis in Section II that the proposed configuration can minimize $\hat{i}_{bi(\max)}$ for the single branch fault condition. Therefore, the configuration proposed by this article is better than the existing one from the point of view of minimizing $\hat{i}_{bi(\max)}$ under this fault condition. As for two branches fault conditions, although the analytical optimal configuration is not derived, the selected analytical configuration is a simple and suboptimal one. Even though the offline optimization method is employed to solve the optimal configuration, the proposed method only needs to solve two undetermined coefficients λ_1 and λ_2 for two branches fault conditions, which is much simpler than the existing methods both in the solving process and the complexity of the optimal coefficients lookup table.

As a whole, compared with the method proposed in [20], the proposed method transfers the problem of branch current configuration into that of solving 8 coefficients but not solving 32 coefficients, which is much easier. And it can directly derive the analytical optimal or suboptimal branch current configurations by preallocating branch current averagely, avoiding solving the optimization equations offline.

IV. Control Scheme

The control scheme of the M3C under branch fault conditions is presented in Fig. 7. In Fig. 7, X represents the identifiers of failed branches, corresponding to that in Section II. For the three reasons aforementioned that may lead to the branch fault, fault detection methods are different. For the case that there are too many failed SMs in one branch, the fault can be detected by counting the number of faulty SMs online and judging whether the remaining SMs are enough to support the input and output voltage. For the latter two cases, i.e., malfunction of SM open-circuit control and mechanical connection failure, the current observation methods proposed in [14] and [15], which are employed to detect the SM open-circuit fault can be utilized to observe branch currents and detect the branch fault by combining with the actual values of branch currents. Once a branch fault is detected and located to branch X, all of the controllable SMs, i.e., the SMs without communication error, in branch X should be blocked to make branch X out of operation. Then, these SMs are operating in the diode-rectifier mode. The capacitor voltages of them will keep fluctuating in a certain range, which is determined by the voltage difference between the input and output nodes. As long as there are enough controllable SMs in branch X, the capacitor voltages of the blocked SMs will not exceed the safe value. At the same time, the current of branch X is almost 0, with only a minuscule component to compensate for the currents of SM discharging resistors, which means branch X is in an equivalent open-circuit state on this condition. Certainly, if there is a mechanical connection failure, branch X is fully open circuit. If each branch is equipped with a circuit breaker, the one in branch X can also be disconnected to remove it from connection and discharge the capacitors in it completely.

Similar to the normal condition, the capacitor voltage balancing control is divided into three levels, i.e., overall energy control, branch energy balancing control, and individual voltage balancing control. It should be noted that when branch X is failed, the capacitor voltages in this branch, i.e., u_{cXj}, are set to their rated value U_C^* to avoid their impact on the overall energy and branch energy balancing control.

First, the overall energy control is employed to control the average value of all SM capacitor voltages to U_C^* , which is

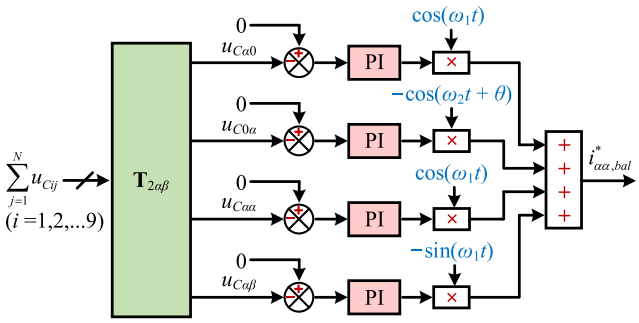

Fig. 8. Closed-loop control scheme of $i^*_{\alpha\alpha,bal}$.

realized by controlling the active current component of the gird-side i^*_{gd}. The reactive current component i^*_{gq} is set to 0 to guarantee the unit power factor.

Second, although the branch energy can be maintained balanced by employing the branch current configurations derived in Section II theoretically, circuit-parameter differences in actual systems can produce additional energy imbalance. Therefore, it is necessary to add closed-loop branch energy control based on the existing branch current distribution to ensure the branch energy balancing in actual systems. The closed-loop branch energy control is realized by employing the method proposed in [23]. This method transfers summation of capacitor voltages of each branch into eight values in the double $\alpha\beta 0$ frame, i.e., $u_{C\alpha 0}$, $u_{C\alpha\alpha}$, etc. Additional circulating currents, i.e., $i^*_{\alpha\alpha,bal}$, $i^*_{\alpha\beta,bal}$, $i^*_{\beta\alpha,bal}$, and $i^*_{\beta\beta,bal}$ are employed to control the eight transferred capacitor voltages to 0 to ensure branch energy balance. The closed-loop control schemes of the four circulating currents are derived according to the relationship between them and the eigth transferred capacitor voltages, with the control scheme of $i^*_{\alpha\alpha,bal}$ presented in Fig. 8 as an example. The derived branch current configurations, such as (11), (27), and (32), are also transferred by double $\alpha\beta 0$ transformation into four circulating currents, i.e., $i^*_{\alpha\alpha(\mathrm{XF\_0})}$, etc. It should be noted that $\cos\varphi_2$ and $\sin\varphi_2$ in the coefficients of i_{c1} and i_{c2} are calculated by transforming the three-phase output currents into *dq*-axis currents by rotating coordinate transformation, with the phase angle of u_r (i.e., $\omega_2 t+\theta$) taken as the angle of coordinate transformation. $i^*_{\alpha\alpha(\mathrm{XF\_0})}$ and $i^*_{\alpha\alpha,bal}$ (the same as the others) are added as the final reference value of circulating currents, as shown in Fig. 7. The control of circulating currents is realized by 4 PR controllers. Each PR controller has two resonance points with frequencies equaling ω_1 and ω_2, which can achieve the accurate tracking of the ac components in the reference value. $v^*_{\alpha\alpha(\mathrm{XF})}$, $v^*_{\alpha\beta(\mathrm{XF})}$, $v^*_{\beta\alpha(\mathrm{XF})}$ and $v^*_{\beta\beta(\mathrm{XF})}$ are circulating voltages in the double $\alpha\beta 0$ frame. They should be transferred into nine values corresponding to each branch by inverted double $\alpha\beta 0$ transformation $\mathbf{T}^{-1}_{2\alpha\beta}$, which is defined as

$$\begin{aligned}
\chi_1 &= \chi_{\alpha\alpha}\\
\chi_2 &= (\sqrt{3}\chi_{\beta\alpha}-\chi_{\alpha\alpha})/2\\
\chi_3 &= -(\chi_{\alpha\alpha}+\sqrt{3}\chi_{\beta\alpha})/2\\
\chi_4 &= (\sqrt{3}\chi_{\alpha\beta}-\chi_{\alpha\alpha})/2\\
\chi_5 &= (\chi_{\alpha\alpha}+3\chi_{\beta\beta}-\sqrt{3}\chi_{\alpha\beta}-\sqrt{3}\chi_{\beta\alpha})/4\\
\chi_6 &= (\chi_{\alpha\alpha}-3\chi_{\beta\beta}-\sqrt{3}\chi_{\alpha\beta}+\sqrt{3}\chi_{\beta\alpha})/4\\
\chi_7 &= -(\chi_{\alpha\alpha}+\sqrt{3}\chi_{\alpha\beta})/2\\
\chi_8 &= (\chi_{\alpha\alpha}-3\chi_{\beta\beta}+\sqrt{3}\chi_{\alpha\beta}-\sqrt{3}\chi_{\beta\alpha})/4\\
\chi_9 &= (\chi_{\alpha\alpha}+3\chi_{\beta\beta}+\sqrt{3}\chi_{\alpha\beta}+\sqrt{3}\chi_{\beta\alpha})/4. \qquad (42)
\end{aligned}$$

For branch fault conditions, $v^*_{\alpha\alpha(\mathrm{XF})}$, $v^*_{\alpha\beta(\mathrm{XF})}$, $v^*_{\beta\alpha(\mathrm{XF})}$, and $v^*_{\beta\beta(\mathrm{XF})}$ are not independent considering the degenerative degrees of freedom. There are only three and two degrees of freedom for eight and seven branch operating conditions, respectively. Thus, one or two of the four circulating voltages needs to be expressed by others. Since the faulty branches are uncontrolled, the relationship among the four circulating voltages can be derived by setting the transferred circulating voltages in these branches to 0. For instance, by setting $v^*_{cir,3(\mathrm{3F})}=0$, $v^*_{\beta\alpha(\mathrm{3F})}$ can be derived as

$$v^*_{\beta\alpha(\mathrm{3F})} = -v^*_{\alpha\alpha(\mathrm{3F})}/\sqrt{3}. \qquad (43)$$

For the two seven-branch operating conditions discussed in Section II, similar results can be derived as

$$\begin{aligned}
v^*_{\alpha\beta(\mathrm{34F})} &= v^*_{\alpha\alpha(\mathrm{34F})}/\sqrt{3}, v^*_{\beta\alpha(\mathrm{34F})} = -v^*_{\alpha\alpha(\mathrm{34F})}/\sqrt{3}\\
v^*_{\alpha\beta(\mathrm{35F})} &= \frac{(2v^*_{\alpha\alpha(\mathrm{35F})}+3v^*_{\beta\beta(\mathrm{35F})})}{\sqrt{3}}, v^*_{\beta\alpha(\mathrm{35F})}\\
&= -v^*_{\alpha\alpha(\mathrm{35F})}/\sqrt{3}. \qquad (44)
\end{aligned}$$

Finally, the phase-shifted carrier (PSC) PWM-based method is employed to guarantee the individual voltage balancing in each branch. This is realized by slightly adjusting the duty ratio of each SM according to capacitor voltages and the direction of branch current.

V. Experimental Results

A. Experimental System

An M3C prototype with 3 SMs in each branch (27 SMs in total) is built to verify the proposed branch fault control method. The circuit diagram of the experimental system and the experimental platform are shown in Fig. 9. Three circuit breakers are connected in series with branch 3, 4, and 5 to completely disconnect the corresponding branch after it is failed. It should be noted that, as mentioned in Section IV, they are not necessarily required to realize the fault-tolerant control of the branch fault, which can be realized by just blocking all controllable SMs in the faulty branch. Two adjustable resistors R_{L1} and R_{L2} are connected in parallel to form the load resistor. A load transformer is connected in series with the load inductor L_{L0} to widely adjust $\cos\varphi_2$ online by changing the equivalent load inductance, which is utilized to verify that the proposed branch current configurations are automatically adaptive to different φ_2. The central controller of the prototype consists of a digital signal processor TMS320F28377 and an

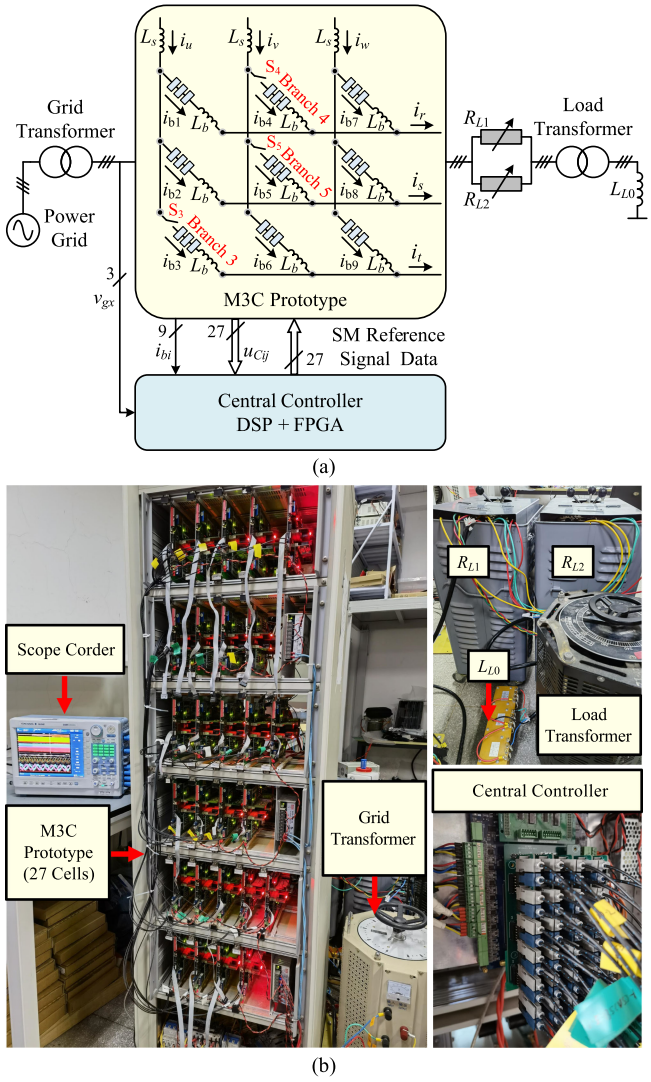

Fig. 9. (a) Circuit diagram of the experimental system. (b) Experimental platform.

field-programmable gate array (FPGA) EP3C25Q240C8, which is utilized to implement the main control algorithm. Each SM has a complex programmable logic device (CPLD) based SM controller to transmit capacitor voltage, receive the reference signal, and realize the modulation of the *H*-bridge circuit. The data of capacitor voltages and reference signals are transmitted between the central FPGA and SM CPLDs by 54 optical-fiber-based serial communication interfaces. Each SM synchronizes the carrier phase by the completion of receiving according to the identifier of the SM. As a result, PSC-PWM is realized. The detailed experimental parameters are summarized in Table I.

B. Experimental Results of Eight-Branch Operating Conditions

Fig. 10 presents the experimental results when branch 3 is failed, including the whole process waveforms, the zoomed waveforms of the branch fault transient state and steady state (from left to right of each line). As presented in the whole process waveforms, the M3C prototype operates normally from t_{10} to

TABLE I
EXPERIMENTAL PARAMETERS

Parameters	Value	Parameters	Value
Rated capacitor voltage	$U_C^* = 120$V	Grid frequency	$f_1 = 50$Hz
SMs per branch	$N = 3$	Grid voltage magnitude	$\hat{v}_{g1} = 120$V
SM capacitance	$C = 880\mu$F	Output frequency	$f_2 = 30$Hz
Branch inductance	$L_b = 2$mH	Output voltage magnitude	$\hat{v}_{m2} = 120$V
AC grid inductance	$L_s = 5$mH	Rated load resistance	$R_{LN} = 15\Omega$
Carrier frequency	$f_s = 2$kHz	Rated load inductance	$L_{LN} = 10$mH

t_{11} with load resistance $R_L = R_{LN}$ and load inductance $L_L = L_{LN}$ ($\varphi_2 = 7.2°$). At the moment t_{11}, assuming that the fault of branch 3 is detected, all SMs in branch 3 are blocked, and circuit breaker S_3 is open to disconnect branch 3. It should be noted that although the detection methods of the branch fault are shown in Fig. 7, the fault detection process is omitted in the experiments of this article. After the moment t_{12}, the load is changed to that $R_L = 16.5\ \Omega$ and $L_L = 35$ mH ($\varphi_2 = 21.8°$) by adjusting the turns-ratio of the load transformer. R_L is also changed because the stray resistances of L_{L0} and the load transformer equivalent to the primary side also increase along with the increment of equivalent inductance. The actual load parameters are derived by the calculated results of $\cos\varphi_2$ and the value of $\hat{i}_{m2}$ after the load is changed.

As seen from the waveforms of capacitor voltages, the proposed method can guarantee the capacitor voltage balance of healthy branches when branch 3 is failed, whatever for the initial rated load or the changed low power factor load, since the coefficients of i_{c1} and i_{c2} can be directly obtained by calculating $\cos\varphi_2$ and $\sin\varphi_2$ online. This proves that "Constraint 2" is satisfied. u_{c31} (the capacitor voltage of the first SM in branch 3) gradually decreases after S_3 is open because there is no energy supplement anymore. From the waveforms of transient state, branch currents and fluctuation components of capacitor voltages both keep symmetrical before S_3 is open, since the M3C prototype operates under the normal condition. After S_3 is open, i_{b3} changes to 0 immediately, and currents of other branches begin to tracking the reference branch currents expressed by (11), which are not symmetrical anymore. At the same time, capacitor voltage fluctuations of several branches become larger. In addition, the transition from the normal to branch 3 fault condition is smooth, without voltage or current spike. From the steady-state waveforms, the grid-side currents, i.e., i_u, i_v, and i_w, are controlled three-phase symmetrically and in phase with gird voltages v_{gu}, v_{gv}, and v_{gw}, which guarantees the unity power factor of the grid side. Meanwhile, the output voltages and currents also keep symmetrical basically. In order to compare the input and output currents before and after the branch fault in the frequency domain, Figs. 11 and 12 present the frequency spectrums of i_u and i_r under the normal and branch

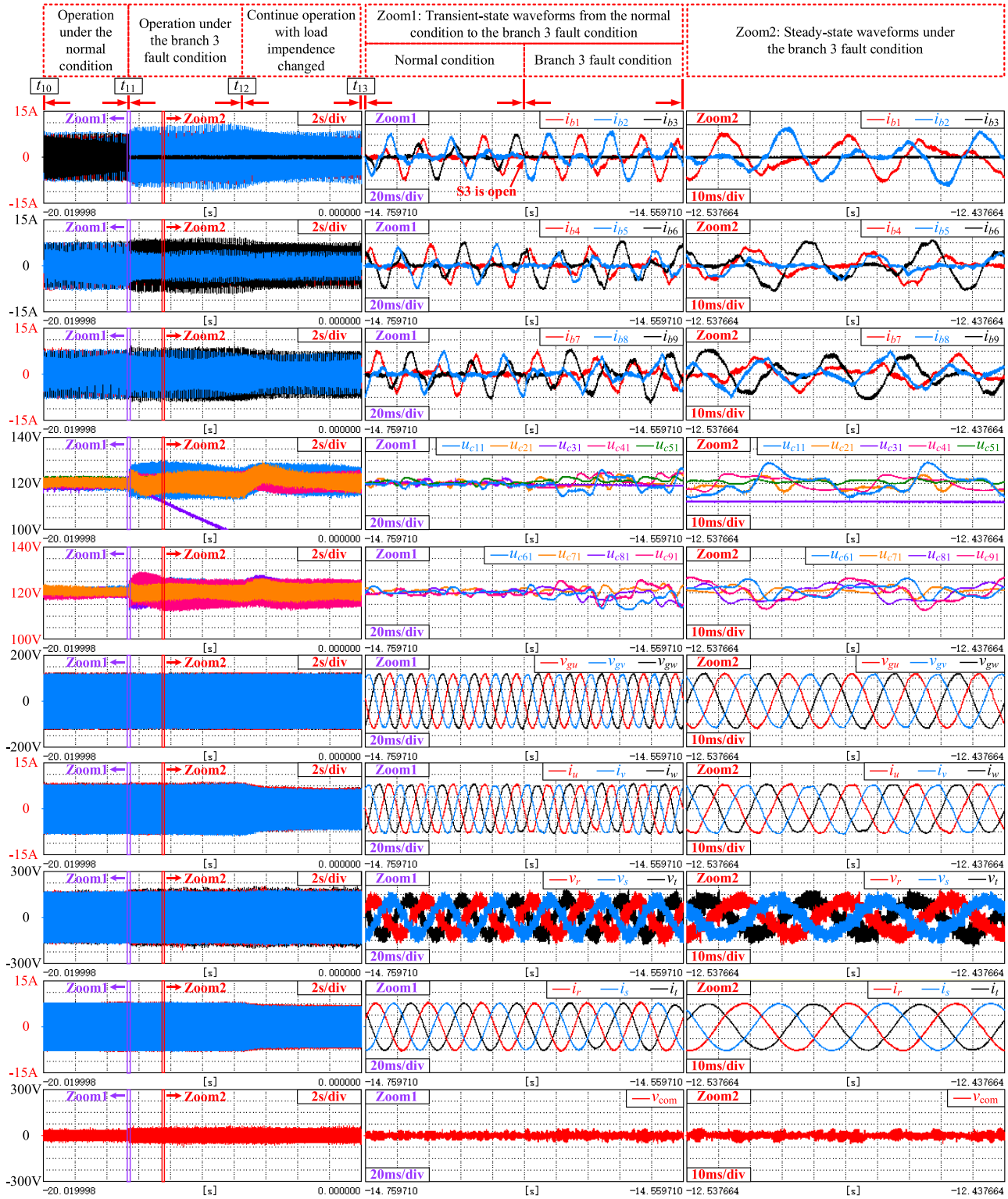

Fig. 10. Experimental results when branch 3 is failed. (From top to bottom: Currents of branch 1 to 3, currents of branch 4 to 6, currents of branch 7 to 9, capacitor voltages of branch 1 to 5, capacitor voltages of branch 6 to 9, ac grid phase-to-neutral voltages, input three-phase currents, output phase-to-neutral voltages, output three-phase currents, and common-mode voltage between input and output neutral points.).

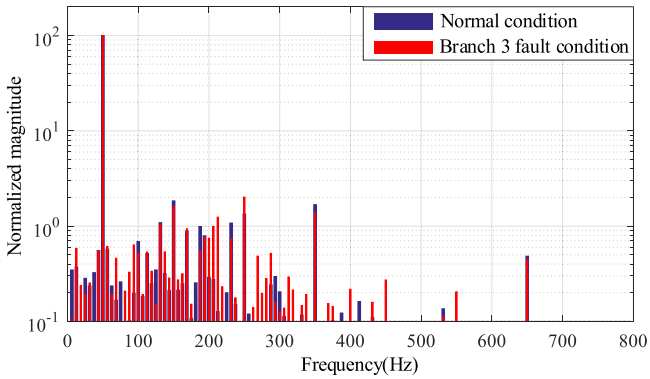

Fig. 11. Frequency spectrum of i_u under the normal and branch 3 fault condition.

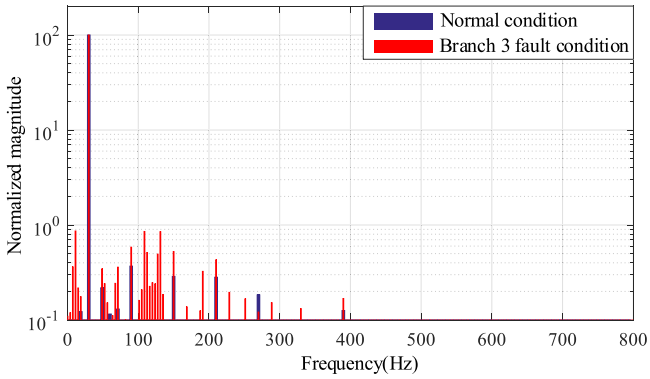

Fig. 12. Frequency spectrum of ir under the normal and branch 3 fault condition.

3 fault condition, respectively. It can be seen that although the amplitudes of several low-order harmonic components in the frequency spectrums of i_u and i_r under the fault condition increase, the increments are relatively minor, which will not bring about significant influences on their total harmonic distortion (THDs). Therefore, the proposed method does not bring about the apparent influence on the input and output currents, i.e., "Constraint 1" is also satisfied. Finally, it can be seen from the waveform of $v_{\rm com}$ that there is no CMV injection after branch 3 is failed.

C. Experimental Results of Seven-Branch Operating Conditions

Fig. 13 presents the experimental results when branches 3 and 4 are failed simultaneously, with the arrangement of waveforms the same as Fig. 10. Similar to Fig. 10, the M3C prototype operates normally from t_{20} to t_{21} with rated load ($\varphi_2 = 7.2°$). At the moment t_{21}, circuit breakers S_3 and S_4 are open to imitate that the simultaneous failure of branch 3 and 4 is detected. After the moment t_{22}, the load is also changed to that $R_L = 16.5\,\Omega$ and $L_L = 35$ mH ($\varphi_2 = 21.8°$). As shown in Fig. 13, the proposed method can ensure the capacitor voltage balance in the whole process, and the input and output currents are also controlled as desired from the zoomed waveforms.

Fig. 14 presents the experimental results when branch 3 and 5 are failed one after another. In Fig. 14, the M3C prototype

TABLE II
THDs AND IMBALANCE FACTORS OF THE INPUT AND OUTPUT CURRENTS UNDER DIFFERENT CONDITIONS

Operating conditions	*THD_i*$_g$	ΔI_g	*THD_i*$_m$	ΔI_m
Normal	4.14%	0.42%	1.32%	0.29%
Branch 3 is failed	4.52%	0.44%	2.25%	1.61%
Branch 3 and 4 are failed	5.28%	0.55%	2.60%	1.51%
Branch 3 and 5 are failed	5.43%	0.43%	2.61%	2.13%

operates normally from t_{30} to t_{31} with rated load ($\varphi_2 = 7.2°$). At the moment t_{31}, assuming that branch 3 is failed, the M3C degenerates to an eight-branch topology. Then, branch 5 is failed at the moment t_{32}, and the circuit continues to degenerate to a seven-branch topology. Compared with the simultaneous failure of two branches, this kind of failure may occur more frequently in practice. As shown in Fig. 14, capacitor voltage balance is ensured in the whole process. Although the waveforms are slightly distorted when compared with the branch 3 fault condition, the steady-state input and output currents are also well controlled. The capacitor voltage fluctuation of this condition is larger than that of the branch 3 and 4 fault condition. The reason is that the relationship between the phase sequence of the input components and that of the output components is different from the branch 3 and 4 fault condition, which lead to different final branch current expressions and capacitor voltage fluctuations. In addition, there is also no CMV injection for the two conditions.

The two experiments prove the effectiveness of the proposed method for seven-branch operating conditions, no matter the failure of two branches occurs simultaneously or successively.

The THDs and imbalance factors of input and output currents under different conditions are shown in Table II to quantitatively compare the control performances of the input and output currents before and after the branch fault. In Table II, *THD_i*$_g$ and *THD_i*$_m$ stand for the THDs of input and output currents, respectively, which are the average values of three-phase THDs. The imbalance factor of input grid currents, ΔI_g, is calculated by (45) according to IEEE std 112-1991, where $I_x\,(x = u, v, w)$ refers to the rms value of the input phase current. Similar expression is employed to calculate the imbalance factor of output currents, i.e., ΔI_m

$$\Delta I_g = \frac{\max\left\{\left|I_u - I_{g\_\rm avr}\right|, \left|I_v - I_{g\_\rm avr}\right|, \left|I_w - I_{g\_\rm avr}\right|\right\}}{I_{g\_\rm avr}}$$

$$I_{g\_\rm avr} = \left(I_u + I_v + I_w\right)/3. \tag{45}$$

According to the results shown in Table II, although *THD_i*$_g$ and *THD_i*$_m$ increase under branch fault conditions, their increments are only about 1.3% even on two branches fault conditions, which is not significant. On the other hand, ΔI_g does not present apparent variations on branch fault conditions, while ΔI_m presents a small increment compared with the normal condition. The main reason is that the input currents are closed-loop controlled, while the output currents are completely open-loop. Therefore, ΔI_m under fault conditions can be improved by employing closed-loop control to the output side.

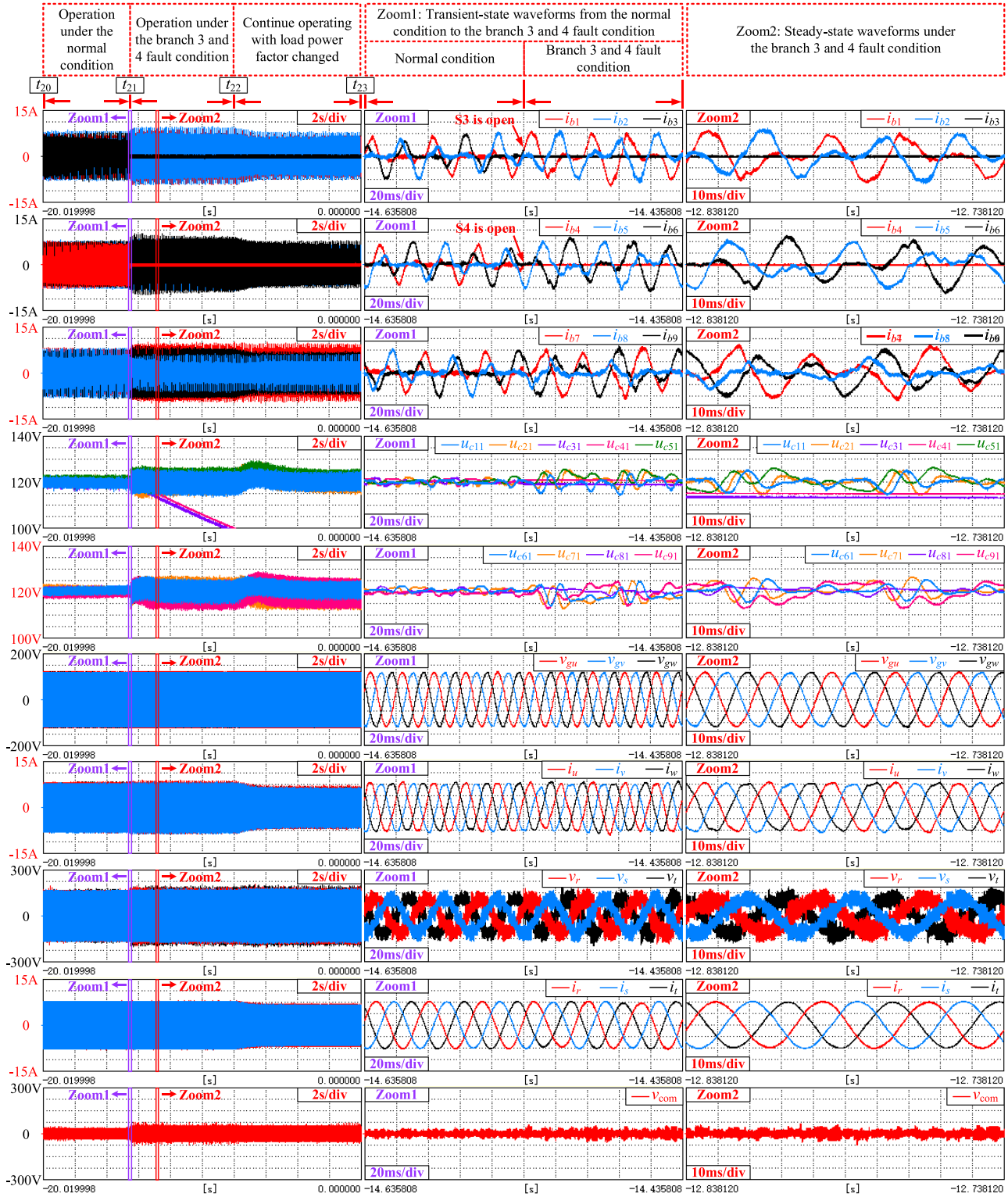

Fig. 13. Experimental results when branch 3 and 4 are failed at the same time. (From top to bottom: Currents of branch 1 to 3, currents of branch 4 to 6, currents of branch 7 to 9, capacitor voltages of branch 1 to 5, capacitor voltages of branch 6 to 9, ac grid phase-to-neutral voltages, input three-phase currents, output phase-to-neutral voltages, output three-phase currents, and common-mode voltage between input and output neutral points.).

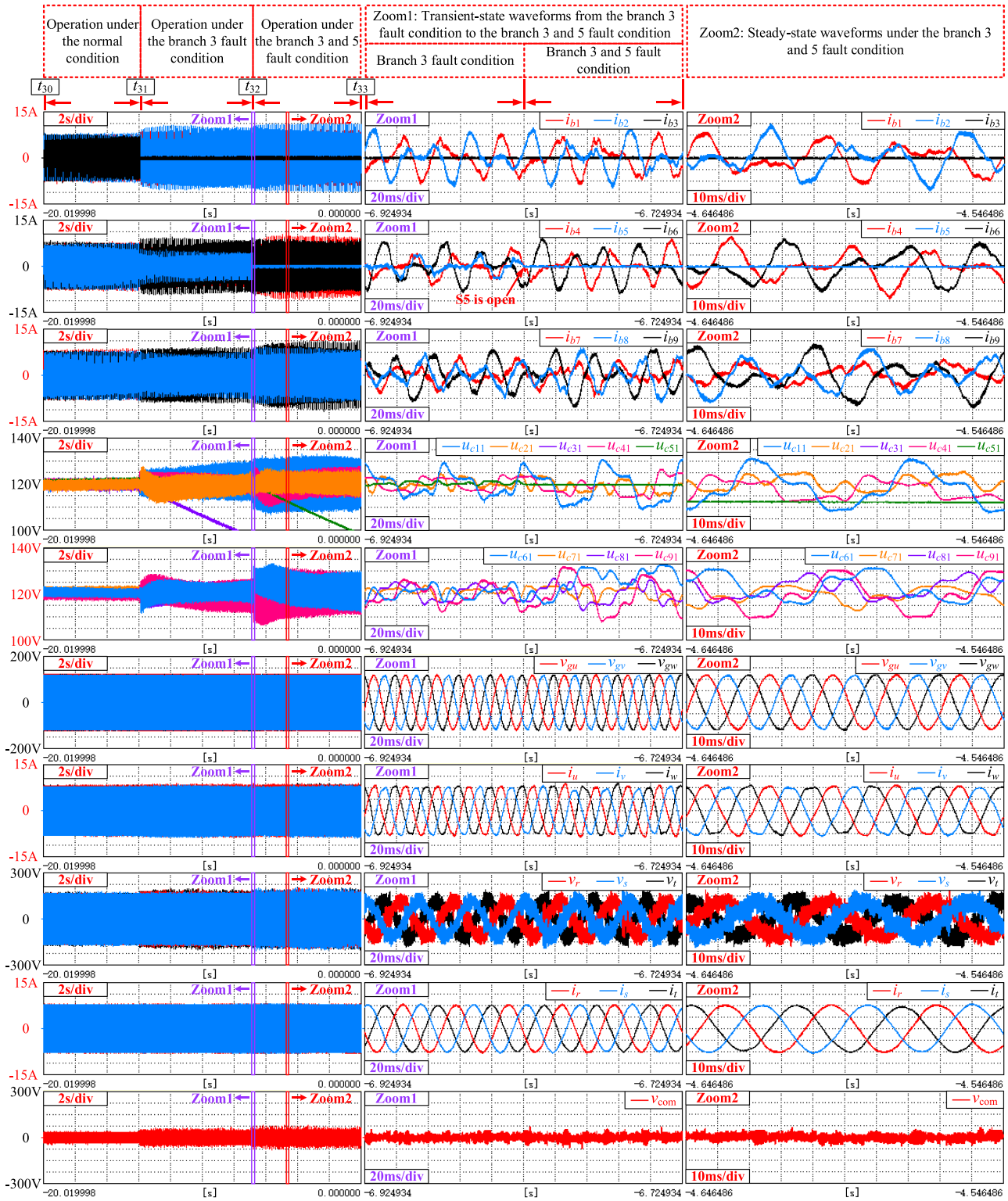

Fig. 14. Experimental results when branch 3 and 5 are failed one after another. (From top to bottom: Currents of branch 1 to 3, currents of branch 4 to 6, currents of branch 7 to 9, capacitor voltages of branch 1 to 5, capacitor voltages of branch 6 to 9, ac grid phase-to-neutral voltages, input three-phase currents, output phase-to-neutral voltages, output three-phase currents, and common-mode voltage between input and output neutral points.).

In conclusion, the proposed branch current configurations do not cause significant influence on the THDs and imbalance factors of the input and output currents whether there is one or two branches failed.

VI. Conclusion

This article proposes a novel branch current configuration method to realize the stable operation of the M3C under branch fault conditions. Both the eight-branch and seven-branch operating conditions are analyzed and verified. According to two primary constraints of the normally operating M3C, the proposed method separates the determination of the optimal branch current configuration into two steps. First, the currents of failed branches are equally allocated to other branches according to the fault conditions and KCL equations of the input and output nodes. Second, the dc power of healthy branches is calculated based on the configuration of the first step. Then, two circulating currents, which contain both the orthogonal input and output current components, are defined and injected into each healthy branch to offset the branch dc power to 0. By solving branch dc power equations, feasible coefficients of the input and output current components in circulating currents are derived. Consequently, the analytical solution of branch current configuration is determined. In terms of minimizing the maximum peak branch current, the derived analytical configurations are optimal for single branch fault conditions and suboptimal for two branches fault conditions. Compared with the existing method, the proposed method transfers the problem of branch current configuration into that of solving 8 coefficients but not solving 32 coefficients, which is much easier. Furthermore, the proposed method can directly derive the analytical optimal or suboptimal results, which are adaptive to different load power factors, avoiding solving configuration coefficients of branch currents offline. The analytical results can also help to derive analytical peak branch currents and capacitor voltage fluctuation in future analysis, which can be utilized to determine the SOA of the M3C under branch fault conditions. Several experiments, one branch is failed, two branches are failed simultaneously, two branches are failed one after another, and changing the load power factor after the branch failure, are carried out on a 27-SM M3C prototype, which verify the effectiveness of the proposed method.

References

[1] H. Akagi, "Classification, terminology, and application of the modular multilevel cascade converter (MMCC)," *IEEE Trans. Power Electron.*, vol. 26, no. 11, pp. 3119–3130, Nov. 2011.

[2] M. A. Perez, S. Bernet, J. Rodriguez, S. Kouro, and R. Lizana, "Circuit topologies, modeling, control schemes, and applications of modular multilevel converters," *IEEE Trans. Power Electron.*, vol. 30, no. 1, pp. 4–17, Jan. 2015.

[3] A. Dekka, B. Wu, R. L. Fuentes, M. Perez, and N. R. Zargari, "Evolution of topologies, modeling, control schemes, and applications of modular multilevel converters," in *IEEE J. Emerg. Sel. Topics Power Electron.*, vol. 5, no. 4, pp. 1631–1656, Dec. 2017.

[4] A. J. Korn, M. Winkelnkemper, P. Steimer, and J. W. Kolar, "Direct modular multi-level converter for gearless low-speed drives," in *Proc. 14th Eur. Conf. Power Electron. Appl.*, Birmingham, U.K., 2011, pp. 1–7.

[5] M. Diaz, E. Ibaceta, A. Duran, C. Melendez, M. Urrutia, and F. Rojas, "Field oriented control of a modular multilevel matrix converter based variable speed drive," in *Proc. 21st Eur. Conf. Power Electron. Appl.*, Genova, Italy, 2019, pp. P.1--P.6

[6] B. Fan, K. Wang, P. Wheeler, C. Gu, and Y. Li, "An optimal full frequency control strategy for the modular multilevel matrix converter based on predictive control," *IEEE Trans. Power Electron.*, vol. 33, no. 8, pp. 6608–6621, Aug. 2018.

[7] S. Liu, X. Wang, Y. Meng, P. Sun, H. Luo, and B. Wang, "A decoupled control strategy of modular multilevel matrix converter for fractional frequency transmission system," *IEEE Trans. Power Del.*, vol. 32, no. 4, pp. 2111–2121, Aug. 2017.

[8] J. Luo, X. Zhang, and Y. Xue, "Small signal model of modular multilevel matrix converter for fractional frequency transmission system," *IEEE Access*, vol. 7, pp. 110187–110196, 2019.

[9] M. Diaz *et al.*, "Control of wind energy conversion systems based on the modular multilevel matrix converter," *IEEE Trans. Ind. Electron.*, vol. 64, no. 11, pp. 8799–8810, Nov. 2017.

[10] N. Thitichaiworakorn, M. Hagiwara, and H. Akagi, "A Medium-voltage large wind turbine generation system using an AC/AC modular multilevel cascade converter," *IEEE J. Emerg. Sel. Topics Power Electron.*, vol. 4, no. 2, pp. 534–546, Jun. 2016.

[11] J. Kucka, D. Karwatzki, and A. Mertens, "AC/AC modular multilevel converters in wind energy applications: Design considerations," in *Proc. 18th Eur. Conf. Power Electron. Appl.*, Karlsruhe, Germany, 2016, pp. 1–10.

[12] M. Vasiladiotis, R. Baumann, C. Häderli, and J. Steinke, "IGCT-based direct AC/AC modular multilevel converters for pumped hydro storage plants," in *Proc. IEEE Energy Convers. Congr. Expo.*, Portland, OR, USA, 2018, pp. 4837–4844.

[13] S. Shao, P. W. Wheeler, J. C. Clare, and A. J. Watson, "Fault detection for modular multilevel converters based on sliding mode observer," *IEEE Trans. Power Electron.*, vol. 28, no. 11, pp. 4867–4872, Nov. 2013.

[14] F. Deng, Z. Chen, M. R. Khan, and R. Zhu, "Fault detection and localization method for modular multilevel converters," *IEEE Trans. Power Electron.*, vol. 30, no. 5, pp. 2721–2732, May 2015.

[15] B. Li, S. Shi, B. Wang, G. Wang, W. Wang, and D. Xu, "Fault diagnosis and tolerant control of single IGBT open-circuit failure in modular multilevel converters," *IEEE Trans. Power Electron.*, vol. 31, no. 4, pp. 3165–3176, Apr. 2016.

[16] J. Kucka, D. Karwatzki, and A. Mertens, "Optimised operating range of modular multilevel converters for AC/AC conversion with failed modules," in *Proc. 17th Eur. Conf. Power Electron. Appl.*, Geneva, Switzerland, 2015, pp. 1–10.

[17] *IEEE Guide for Technology of Unified Power Flow Controller Using Modular Multilevel Converter - Part 1: Functions*, IEEE Standard 2745.1-2019, 2019.

[18] C. Wang, K. Wang, Z. Zheng, B. Yang, K. Sun, and Y. Li, "Analysis and control of three-phase modular multilevel converters under the single arm fault condition," *IEEE Trans. Power Electron.*, vol. 34, no. 9, pp. 8293–8298, Sep. 2019.

[19] D. Karwatzki, M. von Hofen, L. Baruschka, and A. Mertens, "Operation of modular multilevel matrix converters with failed branches," in *Proc. 40th Annu. Conf. IEEE Ind. Electron. Soc.*, Dallas, TX, USA, 2014, pp. 1650–1656.

[20] B. Fan, K. Wang, Z. Zheng, L. Xu, and Y. Li, "Optimized branch current control of modular multilevel matrix converters under branch fault conditions," *IEEE Trans. Power Electron.*, vol. 33, no. 6, pp. 4578–4583, Jun. 2018.

[21] L. Baruschka and A. Mertens, "A new three-phase AC/AC modular multilevel converter with six branches in hexagonal configuration," *IEEE Trans. Ind. Appl.*, vol. 49, no. 3, pp. 1400–1410, May/Jun. 2013.

[22] F. Kammerer, J. Kolb, and M. Braun, "Fully decoupled current control and energy balancing of the modular multilevel matrix converter," in *Proc. 15th Int. Power Electron. Motion Control Conf.*, Novi Sad, Serbia, 2012, pp. LS2a.3–1–LS2a.3–8.

[23] W. Kawamura, M. Hagiwara, and H. Akagi, "Control and experiment of a modular multilevel cascade converter based on triple-star bridge cells," *IEEE Trans. Ind. Appl.*, vol. 50, no. 5, pp. 3536–3548, Sep./Oct. 2014.

Chao Wang (Student Member, IEEE) was born in Gansu, China, in 1993. He received the B.S. degree in electrical engineering in 2016 from the Department of Electrical Engineering, Tsinghua University, Beijing, China, where he is currently working toward the Ph.D. degree.

His research interests include high frequency power converters and the topology and control of multilevel converters.

Zedong Zheng (Senior Member, IEEE) was born in born in Shandong, China, in 1980. He received the B.S. and Ph.D. degrees in electrical engineering from the Department of Electrical Engineering, Tsinghua University, Beijing, China, in 2003 and 2008, respectively.

He is currently an Associate Professor with the Department of Electrical Engineering, Tsinghua University. His current research interests include power electronics converters and high-performance motor control systems.

Kui Wang (Senior Member, IEEE) was born in Hubei, China, in 1984. He received the B.S. and Ph.D. degrees in electrical engineering from the Department of Electrical Engineering, Tsinghua University, Beijing, China, in 2006 and 2011, respectively.

From 2018 to 2019, he was a Visiting Scholar with the Center for Ultra-Wide-Area Resilient Electric Energy Transmission Networks, University of Tennessee, Knoxville, TN, USA. He is currently an Assistant Researcher with the Department of Electrical Engineering, Tsinghua University. His research interests include topology and control of multilevel converters, renewable energy generation, and wide band-gap semiconductor applications.

Bo Yang (Member, IEEE) was born in Shaanxi, China, in 1983. He received the B.S., M.S., and Ph.D. degrees in electrical engineering from the Xi'an University of Technology, Xi'an, China, in 2006, 2009, and 2014, respectively.

Since 2014, he has been a Lecturer with the School of Electrical Engineering, Xi'an University of Technology. His research interests include multilevel converters and power quality control.

Peiyi Zhou (Student Member, IEEE) was born in Xinjiang, China. He received the master's degree in electrical engineering from the Department of Electrical Engineering, Xinjiang University, Ürümqi, China, in 2010. He is currently working toward the Ph.D. degree with the Department of Electrical Engineering, Tsinghua University, Beijing, China.

His research interest includes the topology and control of multilevel converters.

Yongdong Li (Senior Member, IEEE) was born in Hebei, China, in 1962. He received the B.S. degree from the Harbin Institute of Technology, Harbin, China, in 1982, and the M.S. and Ph.D. degrees from the Department of Electrical Engineering, Institut National Polytechnique de Toulouse, Toulouse, France, in 1984 and 1987, respectively.

Since 1996, he has been a Professor with the Department of Electrical Engineering, Tsinghua University, Beijing, China. His research interests include power electronics, machine control, and transportation electrification.